



Biocompatible liquid-crystal elastomers mimic the intervertebral disc

Rajib K. Shaha^{a,*}, Daniel R. Merkel^a, Mitchell P. Anderson^a, Emily J. Devereaux^b, Ravi R. Patel^c, Amir H. Torbati^c, Nick Willett^b, Christopher M. Yakacki^c, Carl P. Frick^a

^a Department of Mechanical Engineering, University of Wyoming, Laramie, WY, 82071, USA

^b Emory University School of Medicine, Decatur, GA, 30033, USA

^c Department of Mechanical Engineering, University of Colorado Denver, Aurora, CO, 80045, USA

ARTICLE INFO

Keywords:

Liquid crystal elastomer
Biomaterial
Intervertebral disc implant
Porous LCE
Biocompatibility
Wettability
Nucleus pulposus
Annulus fibrosus

ABSTRACT

The hierarchical and anisotropic mechanical behavior requirement of load-bearing soft tissues limits the utility of conventional elastomeric materials as a replacement for soft-tissue materials. Liquid-crystal elastomers (LCEs) have the potential to excel in this regard owing to its unique combination of mesogenic order in an elastomeric network. In this study, the mechanical behavior of the LCEs relevant to load-bearing biomedical applications was explored. LCEs with different network orientations (i.e., mesogen alignments) were investigated by fabricating the LCEs with polydomain and monodomain configurations. The polydomain and monodomain LCEs with the same degree of network crosslinking demonstrated diverse mechanical behavior, ranging from highly stiff and elastic nature to high damping capacity, depending on the loading direction with respect to the network alignment. The LCEs were also capable of matching the anisotropic mechanical behavior of an intervertebral disc. Additional studies were conducted on the *in vivo* biological response of LCEs upon subcutaneous implantation, as well as on the effect of the exposure to an *in vitro* simulated physiological environment on the mechanical behavior. The LCEs' mechanical response was negligibly affected when exposed to biomedically relevant conditions. Furthermore, the solid and porous LCEs did not show any adverse effect on the surrounding tissues when implanted subcutaneously in rats. The biological response allows for tissue ingrowth and helps illustrate their utility in implantable biological devices. Finally, the utility of LCEs to mimic the mechanical function of biological tissue such as intervertebral disc was demonstrated by fabricating a proof of concept total disc replacement device.

1. Introduction

Liquid-crystal elastomers (LCEs) consist of stiff mesogenic molecules in a lightly crosslinked polymeric network (Donald et al., 2006; Finckelmann et al., 1981; Kularatne et al., 2017; Ohm et al., 2010; Warner and Terentjev, 2003). This unique structure gives LCEs the ability to demonstrate elastomeric mechanical behavior while possessing liquid-crystalline order. The rotation and alignment of the stiff mesogenic backbone allow the material to exhibit anisotropic mechanical behavior, while the scarce crosslinking permits the material to possess rubber-like elasticity. This coupling of properties gives LCEs many advantageous attributes, including large energy dissipation capacity (Clarke et al., 2001; Merkel et al., 2019), shape-shifting actuation (Ge and Zhao, 2019; Yakacki et al., 2015), and birefringence (Ikeda et al., 2007; Ware et al., 2015). LCEs have been proposed for engineering applications such as actuators (Li et al., 2012), soft robotics (Ge and

Zhao, 2019; Shang et al., 2019), mechanical damping (Clarke et al., 2001; Merkel et al., 2019), optical elements (Brannum et al., 2019; Varanytsia et al., 2015), and more.

LCEs are often categorized into two broad groups, Polydomain and Monodomain, based on the mesogen orientation. These two groups have distinctly independent behavior, and both will be examined through the course of this study. The self-organizing nature of mesogens usually leads to LCEs with localized domains of ordered mesogens, i.e., polydomain LCEs (Azoug et al., 2016; Traugutt et al., 2017; Urayama et al., 2006; Yakacki et al., 2015). Despite the presence of local anisotropy, polydomain LCEs usually possess isotropic mechanical properties on the macroscale because the localized domains lack global alignment (Traugutt et al., 2017; Urayama et al., 2009). When the mesogens are aligned in a prescribed global direction, the LCE is termed to have a monodomain structure and will demonstrate true anisotropic behavior (Merkel et al., 2018; Weilepp et al., 1999). Various techniques, such as

* Corresponding author.

E-mail address: rshaha@uwyo.edu (R.K. Shaha).

<https://doi.org/10.1016/j.jmbbm.2020.103757>

Received 31 December 2019; Received in revised form 23 February 2020; Accepted 28 March 2020

Available online 30 March 2020

1751-6161/© 2020 Elsevier Ltd. All rights reserved.

the application of polarized light (Ware et al., 2015), magnetic fields (Buguin et al., 2006), substrate surface treatment (Li and Keller, 2006), and mechanical stretching (Beyer et al., 2007; Yakacki et al., 2015) have been utilized to align the mesogens. Additionally, the presence of solvent (Boothby et al., 2017; Traugutt et al., 2017), temperature (Beyer et al., 2007; Rožič et al., 2010), and timing (Kularatne et al., 2017) of the mesogen alignment during network formation plays a vital role in locking network in polydomain or monodomain order. Some synthesis schemes fabricate monodomain LCEs in a single step, and mesogens are aligned before the network is formed (Buguin et al., 2006; Thomsen et al., 2001; Ware et al., 2015). The approach used in the current work fabricates monodomain LCEs in two steps. Mesogens are first aligned when the network is partially cured, and then a second stage reaction occurs that completely cures the network and locks in the global alignment (Beyer et al., 2007; Finkelmann et al., 1981; Hiraoka et al., 2008; Kularatne et al., 2017; Yakacki et al., 2015).

In addition to traditional engineering applications, LCEs have been proposed for biomedical applications. These applications include artificial muscles (De Gennes et al., 1997; Ikeda et al., 2007; Li and Keller, 2006), porous tissue-engineering scaffolds (Gao et al., 2016; Martella and Parmeggiani, 2018; Prévôt et al., 2017; Sharma et al., 2015), interbody fusion cage (Volpe et al., 2019), drug delivery vehicle (Inoue et al., 2019), and vascular implants (Ferrantini et al., 2019; Nagahama et al., 2007). Regarding the physical and mechanical characterization of LCEs, the shape-shifting and actuation behavior of LCEs have most commonly been investigated. While a few studies have also reported on the unique damping capacity (Clarke et al., 2001; Merkel et al., 2019) and anisotropic behavior (Merkel et al., 2018; Weillepp et al., 1999) of LCEs, the potential application of this unique material in load-bearing biomedical applications has been largely overlooked.

In biomedical applications, porous materials are often considered desirable as they promote cell-implant interaction, tissue growth, and mass transport between cells and their surroundings (Sharma et al., 2015). A handful of recent studies introduced porous LCE material as a cell culture substrate and tissue engineering scaffold (Bera et al., 2015; Gao et al., 2016; Prévôt et al., 2018, 2017; Sharma et al., 2015). However, these studies did not focus on the mechanical characterization of the porous material. While the properties of porous polymers, in general, are well understood (Avalle et al., 2001; Gibson and Ashby, 1982), it is unclear how the unique soft elasticity of LCEs will influence the behavior and warrants deeper investigation.

Besides the requisite mechanical function, a potential biomedical implant must be created with a material that is compatible with the surrounding tissue upon implantation. Furthermore, the performance of both the material and the implant itself should not degrade after exposure to the biological environment. A few recent *in vitro* studies (Ferrantini et al., 2019; Gao et al., 2016; Sharma et al., 2017) have reported on cytocompatible compositions of LCEs. Moreover, a previous study has demonstrated that LCE materials similar to those utilized in the current work are non-cytotoxic by utilizing evidence from MEM elution and direct contact tests (Yakacki et al., 2015). The research to be presented investigated the *in vivo* subcutaneous response, and how the mechanical behavior of LCEs is affected by physiological conditions.

Degenerative disc disease (DDD) is a widespread medical condition that affects hundreds of thousands of Americans and costs the healthcare system billions of dollars annually (Katz, 2006). Patients with DDD have their intervertebral disc (IVD) degraded, caused by injury or natural aging process (Cortes and Elliott, 2014). Traditionally, the course of treatment is to perform a spinal fusion. Interbody fusion cages make up over half of the total market size and are the most established method for treating disc degeneration; however, these procedures have a high complication rate (36.4%) and often require revision surgery (Chrastil and Patel, 2012). This procedure typically results in a significant reduction in pain at the cost of limited mobility (Huang et al., 2006) and adjacent level disease (Kim et al., 2012; Verma et al., 2013). Alternatively, a total intervertebral disc replacement (TDR) may be implanted

in lieu of a fusion procedure such that maximum mobility and comfort are retained. Unfortunately, both approaches have high rates of subsidence and revision (Chrastil and Patel, 2012). Potential reasons for these high rates of revision include stress shielding due to the stiff materials typically used, migration of the implant, high mechanical stress, and surgical error in implant placement (Kim et al., 2012; Nasto and Logroscino, 2016), (). The high stiffness also inhibits shock absorption across the plastic bearing segment, a crucial property of the IVD (Pham et al., 2015). This lack of energy dissipation across the implant can lead to loosening and premature device failure due to wear and damage (Hyde et al., 2017). It is thus highly desirable to design new implants that better mimic actual biological function, increase mobility, improve implant fixation, and ultimately decrease rates of revision. However, conventional elastomers are unable to adequately mimic the IVD due to IVD's hierarchical structure and highly anisotropic mechanical behavior (Cortes and Elliott, 2014; Nerurkar et al., 2010). The IVD broadly consists of the Annulus Fibrosus and Nucleus Pulposus. The annulus fibrosus is the highly elastic outer region of the IVD, where the most prevalent constituent, collagen fibers, are circumferentially oriented. On the other hand, the nucleus pulposus is the inner gelatinous and viscoelastic core, where the collagen fibers are unorganized. The annulus fibrosus provides structural rigidity while the nucleus pulposus allows cushioning between the vertebrae. Very broad range of mechanical properties of the intervertebral disc are reported in the literature (Cortes and Elliott, 2014; Iatridis et al., 1997b; Nerurkar et al., 2010; Newell et al., 2017). The elastic modulus of the nucleus pulposus ranges between 0.05 – 0.1 MPa, while the annulus fibrosus ranges from 0.1 to 1 MPa, depending on the health of the tissue and testing method (Nerurkar et al., 2010). The LCEs have been reported to show storage modulus in the similar range of 0.1 – 2 MPa (Merkel et al., 2018; Saed et al., 2017; Traugutt et al., 2017). Additionally, the $\tan \delta$ of the nucleus pulposus is in the order of 0.2 – 0.7 (Iatridis et al., 1997b) and the LCEs are capable of showing $\tan \delta$ of similar magnitude over a broad temperature range. Besides the similar extent of these mechanical properties, the anisotropic behavior of LCEs can potentially be utilized to devise a functional synthetic IVD.

The driving hypothesis of this study is that the unique, and tailorable properties of LCEs make the class of materials a strong candidate for use in load-bearing biomedical applications and implants. In pursuit of this hypothesis, the investigation was guided by three fundamental questions.

1. Is the mechanical behavior for LCEs relevant to load-bearing biomedical applications?
2. What is the *in vivo* subcutaneous response of solid and porous LCEs, and how is the mechanical behavior affected by exposure to physiological conditions?
3. Can the inherent anisotropy of LCEs be utilized to better mimic the actual biological function in a proof of concept, total disc replacement device?

This study will attempt to elucidate answers to each of these questions by examining the relevant properties of several groups of LCE materials: solid polydomain, porous polydomain, and solid monodomain.

2. Materials and methods

2.1. Synthesis methods

This study employs a facile fabrication method developed by Yakacki et al. in order to create large polydomain and permanent monodomain LCE samples (Saed et al., 2016; Traugutt et al., 2017; Yakacki et al., 2015). A polydomain LCE network with prominent soft elasticity is formed through Michael Addition reactions of a stoichiometric mixture of diacrylate mesogen monomers, di-thiol flexible spacers, and tetra-thiol crosslinkers. A permanent monodomain LCE is made from

bulk polydomain LCE with acrylate functional groups in excess of the stoichiometric amount. The polydomain LCE with excess acrylate is mechanically stretched to align the mesogens and subsequently made permanent by radical photopolymerization of the excess acrylate groups. Owing to the independence of Michael-Addition and radical photopolymerization, this fabrication scheme allows distinct control over the fabrication of both nematic polydomain and monodomain LCE samples.

The LCE samples were synthesized using thiol-acrylate Michael addition and radical photopolymerization following a method adapted from literature (Merkel et al., 2019; Yakacki et al., 2015). Mesogen 1,4-Bis-[4-(3-acryloyloxypropoxy)benzoyloxy]-2-methylbenzene (RM257) was purchased from Wilshire Technologies, Inc. (Princeton, NJ, USA). All other chemicals: bifunctional linear spacer 2,2-(ethylenedioxy) diethanethiol (EDDET), tetra-functional crosslinker pentaerythritol tetrakis (3-mercaptopropionate) (PETMP), base catalyst triethylamine (TEA), inhibitor 2,6-di-tert-butyl-4-methyl phenol (BHT) and photoinitiator 2-hydroxy-4'-(2-hydroxyethoxy)-2-methylpropiophenone (HHMP) were obtained from Sigma-Aldrich, Inc. (St. Louis, MO, USA). The chemicals were used as received from the vendors without further purification.

In this study, LCE samples with two different domain configurations were fabricated: polydomain (PD) and monodomain (MD). For the solid polydomain LCE (PD-solid), the network was formed by a Michael Addition reaction between acrylate functional groups from RM257 and stoichiometric amounts of thiol functional groups, contributed by EDDET and PETMP (Fig. 1). The fabrication started with the melting of RM257 and BHT (1.5 wt. %) at 120 °C in a forced-air oven, followed by thoroughly mixing with EDDET, PETMP and TEA (Fig. 2). The amount of crosslinking was 15 mol%, indicating that 15% of all the thiol functional groups were contributed by the tetra-functional thiol crosslinker (PETMP). TEA was used as the catalyst for the reaction and BHT inhibitor was used to control the reaction rate to allow enough time for casting the solution into molds. The BHT (1.5 wt. %) and TEA (0.33 wt. %) amounts were calculated with respect to the total amount of acrylate and thiol monomers. The LCE mixture was degassed under 22 in-Hg

vacuum until all the dissolved air bubbles were removed and transferred into molds made with glass slides separated by Teflon spacers. The Michael Addition reaction continued at room temperature for 12 h as the mesogens self-assembled into a nematic polydomain configuration. Opaque, solid polydomain LCE (PD-solid) film samples with dimensions of $25 \times 5 \times 1 \text{ mm}^3$, and cylindrical samples with 10 mm diameter by 10 mm height were fabricated.

Porous polydomain LCE (PD-porous) samples were fabricated using a salt leaching technique by adding salt crystals to the LCE forming mixture (Fig. 2). NaCl salt crystals of 250–420 μm size were sieved (US standard sieve series, IL, USA) from mixed sized crystals obtained commercially (Sigma-Aldrich, Inc.). The LCE forming solution, prepared as described above for the solid polydomain material, was mixed with salt crystals at a 1:2 LCE to salt weight ratio using a stainless-steel mixing rod. The mixture was transferred to glass molds with Teflon spacers and allowed to react for 12 h at room temperature. The salt loaded polydomain LCE samples were extracted from the molds and placed in an ultrasonication bath of deionized water (Branson 1510, Branson Ultrasonics, CT, USA). The water was changed every 8 h until all the salt particles were dissolved. The porous polydomain samples were dried in a forced-air oven at 100 °C for 3 h, followed by additional drying in a vacuum oven at 70 °C for 3 h. Porous polydomain film samples with $25 \times 5 \times 2 \text{ mm}^3$ dimensions and cylindrical samples with 10 mm diameter by 10 mm height were fabricated.

The solid monodomain LCE samples were fabricated using a slightly different composition than the solid polydomain material. All monodomain samples were fabricated using 5% in excess of the stoichiometric amount of acrylate functional groups relative to the thiol groups, and a photoinitiator (0.5 wt. % of total acrylate and thiol-containing monomers) was added to the reaction mixture. The Michael Addition reaction took place at an elevated temperature (100 °C), well above the isotropic transition temperature, such that mesogens were randomly oriented while the LCE network was curing and no localized domain structure was present. The reference isotropic transition temperature was taken from reports by other researchers for very similar LCE chemistries (Traugott et al., 2017). After the polymer network was fully cured, the

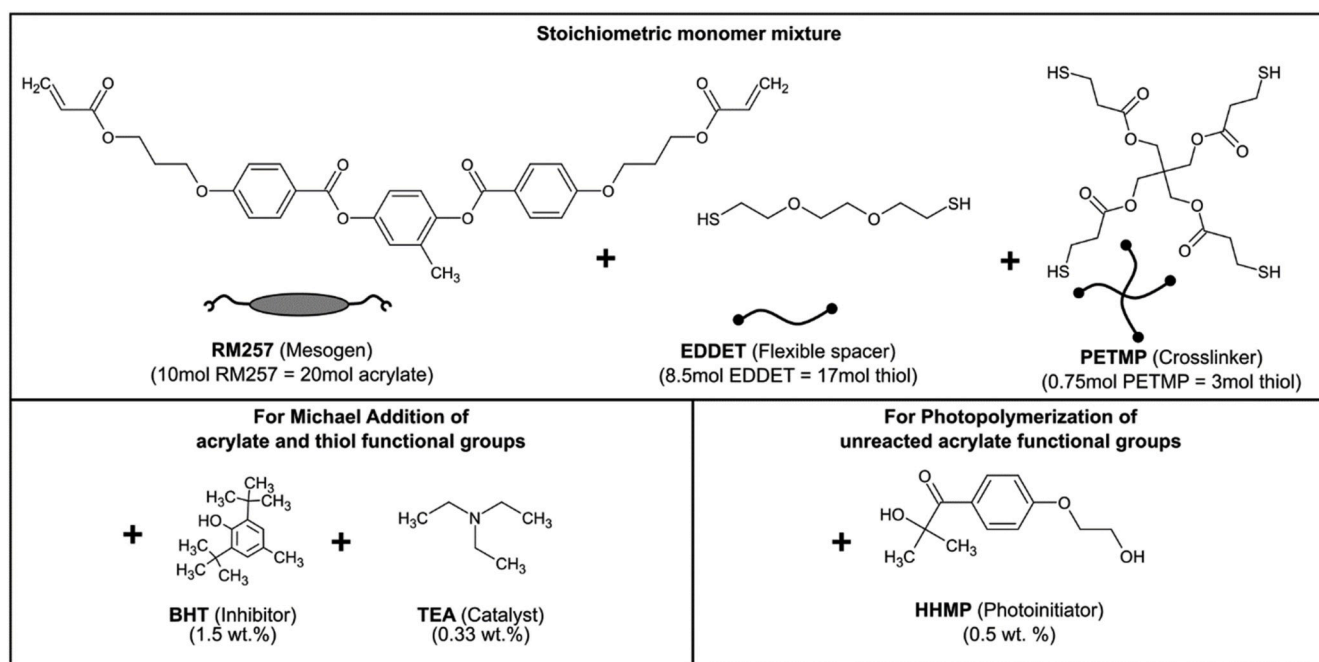


Fig. 1. The chemical structure of the liquid crystalline elastomer (LCE) constituents shown schematically. Diacrylate-mesogen (RM257), dithiol-flexible chain (EDDET), tetrathiol-crosslinker (PETMP) are reacted via Michael-addition reaction with base catalyst (TEA) and inhibitor (BHT) to obtain polydomain LCE. In order to make monodomain LCE, photoinitiator (HHMP) is added for subsequent radical polymerization of unreacted acrylate functional groups. All chemicals purchased from commercial suppliers and used in as-received condition.

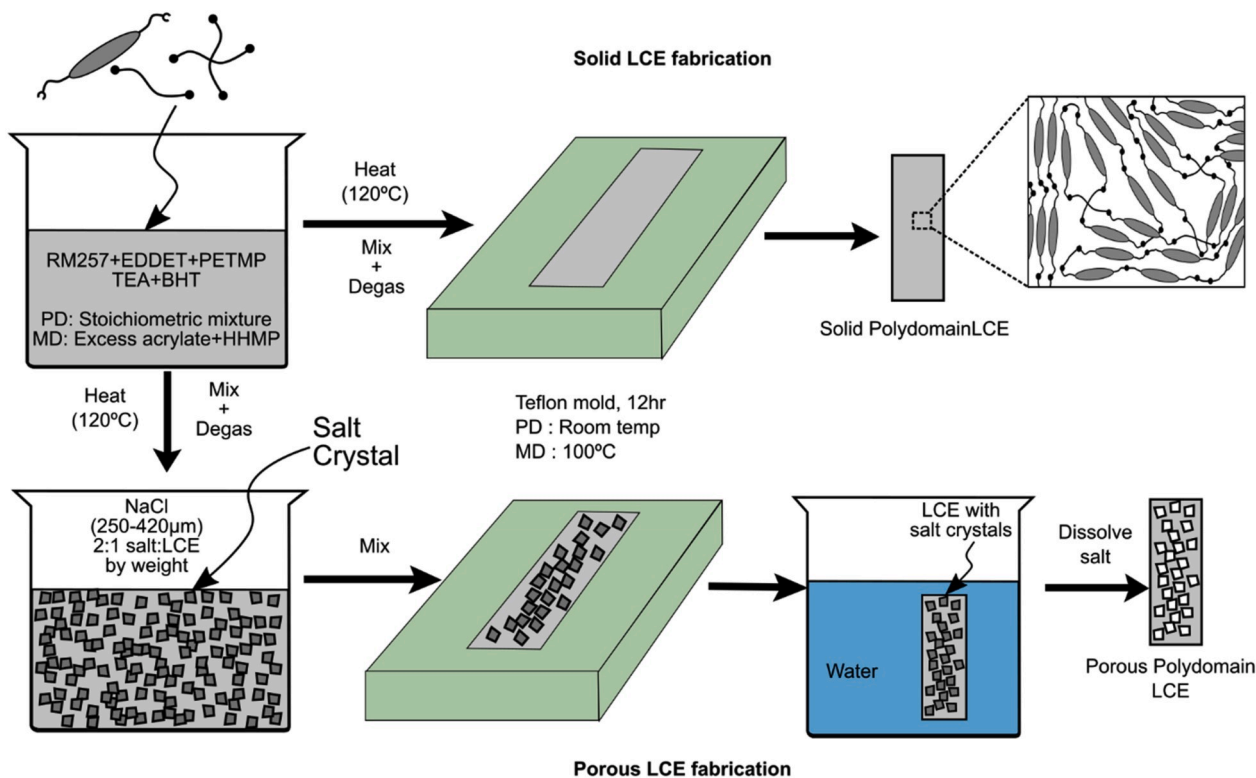


Fig. 2. Schematic diagram describing the fabrication methods for solid and porous polydomain LCE samples. The RM257, EDDET, PETMP, TEA, BHT and HHMP are mixed together and then heated to start the Michael Addition reaction. The mixture is poured into a Teflon mold and kept either at room temperature for the nematic genesis of polydomain materials (PD), or 100 °C for the isotropic genesis of monodomain materials (MD). In order to create porous LCE, salt crystals are added to the mixture early in the process, and ultimately dissolved out in the water after curing of the network has completed.

LCE sample was cooled to room temperature. The cooling allowed the mesogens to reform to a nematic polydomain configuration, which was optically opaque. Critically, the sample had excess unreacted acrylate functional groups. To force the monodomain state, the solid sample was mechanically stretched until it became transparent, termed as clearing strain, indicating the global alignment of the mesogens. This state was temporary until exposure to 365 nm wavelength ultraviolet light (Blackray B-100A/R, UVP, Upland, CA, USA) for approximately 1 h. The ultraviolet irradiation decomposed the photoinitiator to initiate radical photopolymerization, and the excess acrylate functional groups reacted

with each other to fix the stretched shape. This process resulted in a permanent monodomain LCE (Fig. 3). The solid monodomain samples were cut either parallel or perpendicular to the mechanically stretched direction, i.e., the direction of mesogen alignment. The solid monodomain samples were fabricated exclusively to study the anisotropic mechanical behavior of LCEs. Monodomain samples for mechanical testing were termed as “longitudinally” loaded (where loading direction is aligned with the mesogen orientation) or “transversely” loaded (where loading direction is perpendicular to the mesogen orientation) monodomain samples (appearing as “MD-long” or “MD-trans” in the

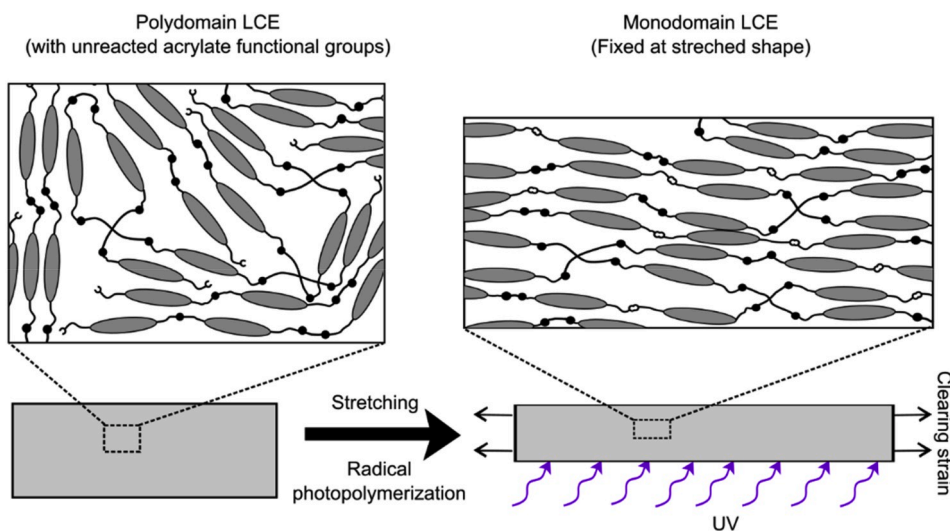


Fig. 3. Schematic diagram of monodomain solid LCE fabrication. Polydomain solid LCE sample with unreacted acrylate functional groups is stretched to clearing strain and photopolymerized with photoinitiator (HHMP) and UV light to create monodomain solid LCE fixed at the stretched shape.

corresponding figures). Monodomain film samples with dimensions of either $25 \times 5 \times 0.85 \text{ mm}^3$ or $8 \times 8 \times 8 \text{ mm}^3$ were prepared.

2.2. Physical characterization

Porous polydomain samples were scanned using a 3D X-ray microscope equipped with two-stage magnification technology (Xradia 520 Versa, Carl Zeiss Microscopy, LLC, Jena, Germany). Cylindrical samples were placed on a rotating stage and projection X-ray images were acquired from various orientations. The samples were scanned using 0.4X, 4X and 20X objectives, to obtain images with $12 \mu\text{m}/\text{voxel}$, $3 \mu\text{m}/\text{voxel}$ and $0.74 \mu\text{m}/\text{voxel}$ resolutions, respectively. The raw images were processed using Dragonfly Pro software provided by the microscope manufacturer to obtain porosity, 3D views and 2D sectional views. The porosity of porous polydomain samples was also measured by comparing the densities of the solid and porous materials. The mass and physical dimensions were measured for three samples each of the porous and solid polydomain materials. The density was calculated as the ratio of the mass and volume and the porosity was subsequently calculated using the following equation.

$$\text{Porosity} = \left(\frac{\rho_s - \rho_p}{\rho_s} \right) \times 100\%$$

ρ_s : Density of solid LCE

ρ_p : Density of Porous LCE

The wettability of both solid and porous polydomain LCEs, and solid monodomain LCEs was assessed by measuring the static water contact angle. The samples were cleaned with isopropyl alcohol for 30 s in an ultrasonication bath, followed by additional cleaning in deionized water for 5 min. The cleaned samples were dried in a vacuum oven at 70°C for 3 h and allowed to cool to room temperature in airtight petri dishes. The surface wettability was measured using a drop shape analyzer (DSA25, Kruss GmbH, Hamburg, Germany). Film samples were placed on a horizontal stage and a $2 \mu\text{l}$ droplet of ultrapure water (Milli-pore Direct-Q, MilliporeSigma, MA, USA) was dispensed onto the sample surface through a 23-gauge needle. The profile of the sessile droplet was imaged within approximately 60s of dispensing using the equipped camera and a circle was fit to the droplet profile. The contact angle was measured as the angle between the water-sample surface and the water-air surface. For each type of LCE, approximately ten measurements were recorded.

2.3. Mechanical testing

Uniaxial tensile tests were performed on all samples (solid and porous polydomain, monodomain tested longitudinally and transversely) using a dynamic mechanical analyzer (DMA Q800, TA Instruments, New Castle, DE, USA). Solid polydomain samples with dimensions of $25 \times 5 \times 1 \text{ mm}^3$, porous polydomain samples with dimensions of $25 \times 5 \times 2 \text{ mm}^3$ and solid monodomain samples with dimensions of $25 \times 5 \times 0.85 \text{ mm}^3$ were held isothermal for 5 min at 37°C before loading to ensure thermal equilibrium. A preload of 0.01 N was applied to remove any slack in either the samples themselves or the load train. Samples were loaded at a strain rate of 1%/s up to 120% strain.

To complement the tensile testing, compression testing was performed on all groups of samples (solid and porous polydomain and monodomain tested longitudinally and transversely). Solid and porous polydomain materials were tested using cylindrical samples with 10 mm diameter \times 10 mm height. Monodomain materials were tested using cubic samples with dimensions of $8 \times 8 \times 8 \text{ mm}^3$. All samples were preloaded to 0.05 N to ensure positive contact with the compression platens. Samples were held isothermal for 10 min at 37°C before loading to ensure thermal equilibrium. All compression tests were performed at a constant strain rate of 1%/s on a second dynamic mechanical analyzer

with a higher maximum load capacity (ElectroForce 3200, TA Instruments, New Castle, DE, USA), than DMA Q800.

Compression testing was also performed on human intervertebral disc (IVD) samples obtained from a donor cadaver (75yr, female). Approximately $10 \text{ mm} \times 10 \text{ mm}$ intervertebral disc samples were obtained from the nucleus pulposus (tissue at the inner core), and annulus fibrosus (tissue at the outer region) (Cortes and Elliott, 2014). The samples were tested in ambient conditions and loaded at a moderate strain rate of 2.5%/s using the ElectroForce DMA 3200. In order to directly compare with the intervertebral disc, additional compression tests were duplicated for LCE materials. Solid polydomain LCE, and longitudinally and transversely loaded monodomain LCEs were tested at identical test temperature and loading rate as the IVD samples. The porous polydomain LCE was not considered as a candidate material to mimic IVD due to their much lower stiffness compared to their solid counterpart, as observed in the initial compression tests. Therefore, additional compression tests were not conducted on the porous LCEs for comparison with the IVD.

The damping behavior of solid polydomain samples was studied under dynamic shear loading using the DMA Q800. This type of test was selected so that results could be directly compared with literature data for the nucleus pulposus reported by Iatridis et al. (1997a). A standard configuration for polymer shear testing was utilized involving two $8 \times 8 \times 4 \text{ mm}^3$ samples sandwiched between an actuated plate at the middle and fixed plates on the outsides. The resulting sample and test fixture configuration was fixed-plate/sample/moving-plate/sample/fixed-plate sandwich. A 10% compressive strain was applied to each sample by adjusting the fixed plates to ensure no slippage during shear loading. An oscillating shear strain of 0.15% was applied at various frequencies between 0.01 Hz to 100 Hz while the viscoelastic damping parameter $\tan(\delta)$ was tracked by the instrument. The strain amplitude was selected from preliminary experiments such that the sample deformation was limited to the linear viscoelastic region.

For all mechanical testing, the force and displacement were tracked by the testing instrument, and engineering stress and strain were calculated using the original sample geometry. Before any subsequent testing of same sample, samples were heated beyond the isotropic transition temperature (100°C), and then allowed to cool back to ambient such that any residual deformation from previous tests was recovered.

2.4. Testing for exposure to physiological conditions

The mass gain of solid polydomain samples was investigated, as the representative LCE material, by exposure to simulated physiological conditions. The porous LCE was excluded from the mass gain study as the porous samples would trap a much larger amount of water compared to the absorbed amount, hence would make the measurement irrelevant. Three solid polydomain films with approximately $25 \times 5 \times 1 \text{ mm}^3$ dimensions were weighed and then left submerged in phosphate-buffer saline (PBS) solution. The PBS solution had a pH of 7.4, prepared by dissolving one tablet (P4417, Sigma-Aldrich) in 200 mL distilled water. The submerged samples were kept at 37°C and shaken at 60 rpm using a shaker table-incubator (Biomega Incu-Shaker Mini, Benchmark Scientific, NJ, USA). The samples were taken out after different soaking durations, and the current mass was recorded before placing the samples back into a fresh PBS solution. The mass gain was calculated using the following equation.

$$\text{Mass gain} = \frac{m_f - m_i}{m_i} \times 100 \%$$

m_i : Initial mass

m_f : Mass on a corresponding day

In order to study the effect of exposure to physiological conditions on

the mechanical behavior, solid polydomain samples soaked for 21 days were also tested in uniaxial tensile loading. The soaked samples were removed from the 37 °C PBS solution immediately before testing and held isothermal at 37 °C for only 2 min to minimize dehydration. The preload and strain rate were same as the tensile testing of the pristine samples. However, contrasting with the pristine samples, the soaked samples were held at 37 °C for at least 24 h in PBS solution before any subsequent testing of same sample to recover any residual deformation, while the possibility of dehydrating the samples is minimized.

The effect of water mass gain on creep behavior was also investigated for solid polydomain LCE samples, before and after soaking. Creep tests were performed on $25 \times 5 \times 1$ mm³ samples using the DMA Q800 by rapidly applying a force and then holding that force constant for 5 min while tracking the strain as a function of time. The creep response of pristine polydomain samples, and samples soaked for 21 days, was compared at stresses of 25 kPa and 100 kPa. All tests were performed at body temperature (37 °C) after samples reaching thermal equilibrium.

2.5. *In-vivo* biocompatibility testing

To investigate one aspect of biological compatibility, solid and porous polydomain LCE materials were subcutaneously implanted in rats. Semi-circular discs of 12 mm diameter were obtained from 1 mm thick solid, and 2 mm thick porous polydomain films. The samples were cut in half to form a semicircle shape, then sterilized in an autoclave before subcutaneous implantation on the chest of three male Sprague Dawley rats 5–6 weeks in age. One animal had four implants (two solid and two porous polydomain samples), while the other two animals had only two implants each (one solid and one porous). The animals were euthanized, and samples removed after four weeks. The recovered samples were stained with Hematoxylin-Eosin (H&E) staining and Mason's trichrome staining (Sigma-Aldrich, St. Louis, MO). The images were obtained with the Axio Observer Z1 microscope (Carl Zeiss, Jena, Germany) and captured using the Axio Vision software (Carl Zeiss Micro Imaging, Thornwood, NY, USA).

3. Results

3.1. Physical characterization

Initial characterization of the relevant materials included measures of porosity and wettability. Porosity was assessed utilizing X-ray microscopy; images of a representative porous polydomain sample are illustrated in Fig. 4. Light gray areas of the images indicate dense material, while dark gray areas indicate pores. The pore structure and distribution are representative of an open cell interconnected porous network. The size of the pores was reflective of the size of salt crystals used (250–420 μm), while the shape of the pores was irregular, and no global alignment was observed. The porosity of the LCE sample was estimated at 54%, calculated using the X-ray microscope instrument manufacturer's image processing software.

Porosity was additionally calculated using traditional gravimetric methods. The average density of solid polydomain LCE was 1252 kg/m³, while the average density of porous polydomain LCE was 568 kg/m³. The resulting calculated porosity was 55%, in very close agreement with measurements made using X-ray imaging.

The wettability of solid and porous polydomain LCE materials and solid monodomain LCE materials was determined by measuring the static water contact angle. The average water contact angle for solid polydomain samples was 84.3°, while the average contact angle for porous polydomain samples was 85.2°. The solid monodomain samples showed an average water contact angle of 87.3°. These water contact angles indicate that all materials are slightly hydrophilic.

3.2. Mechanical behavior

The mechanical response of LCEs can be generally classified into three distinct modes of deformation. The mechanisms for each of these subsequent modes are most readily apparent in solid polydomain materials loaded in tension (Fig. 5). The initial response of the applied tensile load is nearly linear elastic. This is commonly attributed to polymer chains sliding and uncoiling, similar to traditional elastomers.

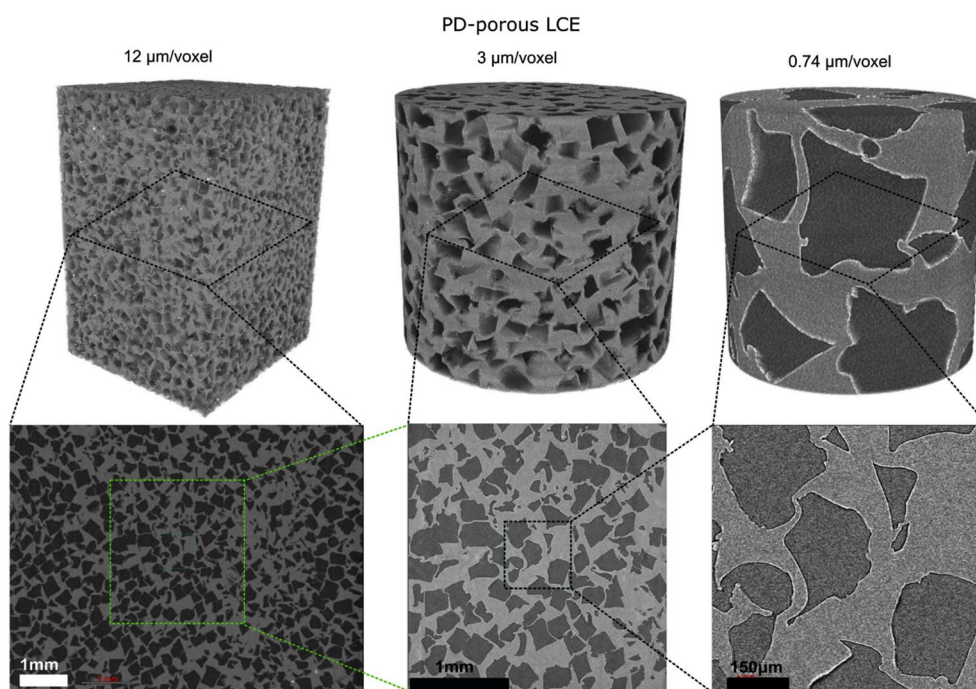


Fig. 4. Three-dimensional X-ray microscopy image of porous polydomain LCE shows the dispersion and shape of the pores. The dissolved-out salt crystals left a continuous network of voids in the material with thin and discontinuous LCE struts. The images were obtained at three different magnifications: 12 μm/voxel, 3 μm/voxel and 0.74 μm/voxel. The volume fraction of the pores was measured to be 54%.

The second mechanical response initiates beyond a critical stress; this deformation mode results in a large plateau region often termed soft elasticity. Within this regime, the microscopic domains of locally aligned mesogens rotate in response to the applied load. Ultimately, the domains continue to rotate until global alignment is achieved, effectively resulting in a non-permanent monodomain structure. The rotation of these mesogen domains allows the material to deform at a nearly constant stress resulting in very efficient energy absorption and dissipation. The final, and subsequent mode of deformation is the elastic stretching of the fully aligned polymer network and monodomain structure. This results in monotonically increasing stress with further deformation until failure, mimicking the behavior once again of a conventional elastomer.

The tensile and compressive behavior for both solid and porous polydomain LCE materials is depicted in Fig. 5. The solid material tested in tension clearly exhibits the three fully developed modes of deformation defined in the previous paragraph. In compression, the solid material initially exhibits the same elastic response as the tensile behavior with an estimated modulus of 680 kPa. Beyond 2.5% strain, the tensile and compressive behaviors quickly diverge. In tension, bulk rotation of the mesogen domains toward the tensile axis results in soft elasticity indicated by a stress plateau. In compression, the mesogens tend to align with the plane perpendicular to the applied load. However, any soft-elastic effect due to mesogen reorientation is overshadowed by the increase in the cross-sectional area of the material, causing a rapid increase in modulus.

The porous material, when compared to the solid material, is much softer in both tension and compression. The tensile and compressive behavior of the porous material is nearly identical for the first 20% of deformation with an estimated modulus of 75 kPa. In tension, the porous material deforms almost linearly with the load. This is contrary to the soft-elastic tensile response of the solid material and assumed to be a result of the collapse and stretching of the porous structure originating from bending and small deformation of the pore struts, rather than rotation of the mesogen domains. In compression, the porous material exhibits typical foam densification behavior beginning at approximately 30% strain.

The uniaxial mechanical responses for solid monodomain LCE samples loaded both longitudinally and transversely, in tension and compression are represented in Fig. 6. Samples loaded longitudinally in

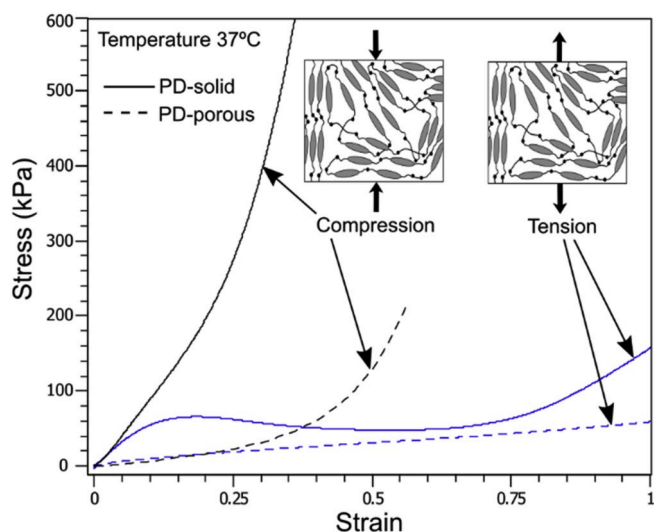


Fig. 5. Representative tensile and compressive mechanical responses for both solid and porous polydomain LCEs. Results show stiffer and stronger behavior under compression. Only the solid polydomain material loaded in tension exhibited a characteristic plateau associated with soft elastic behavior. All the samples were tested at 37 °C and 1% s^{-1} .

tension, and samples loaded transversely in compression, demonstrated only linear stress-strain behavior; no soft-elastic plateau was present (Fig. 6a). In contrast, samples loaded transversely in tension, and samples loaded longitudinally in compression both exhibit soft elasticity (Fig. 6b). This effect is most pronounced for the samples loaded transversely in tension, with a critical stress of approximately 160 kPa and a plateau region extending to nearly 110% strain. The soft-elastic effect was diminished in the samples loaded longitudinally in compression with a critical stress of approximately 60 kPa and extending to about 25% strain. Samples loaded longitudinally in both tension and compression had an initial elastic modulus of 1,100 kPa. Samples loaded transversely in both tension and compression were stiffer, with an initial elastic modulus of 2,300 kPa.

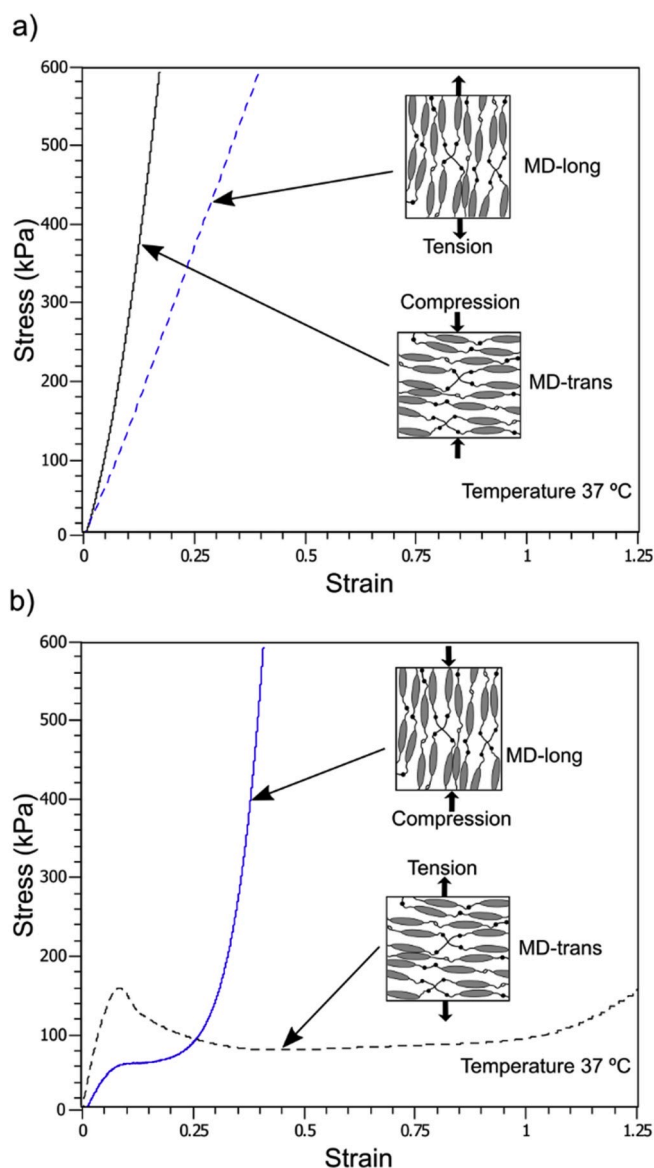


Fig. 6. Representative tensile and compressive mechanical responses for solid monodomain LCE loaded both longitudinally and transversely-a) Monodomain LCEs loaded longitudinally in tension and transversely in compression shows linear elastic behavior, and b) Monodomain LCEs loaded longitudinally in compression and transversely in tension demonstrated the soft-elastic effect. All the samples were tested at 37 °C and 1% s^{-1} .

3.3. Response to physiological condition exposure

The effect of simulated physiological conditions on the mechanical behavior of LCEs was investigated by uniaxial tension and creep testing before and after exposure. The mass gain of solid polydomain samples due to swelling was studied by submerging the material in a PBS solution held at 37 °C. The plot of the average sample mass gain against the soak time is shown in Fig. 7a. The mass increased approximately logarithmically with respect to soaking time until reaching a steady-state value of about 2.5 wt. % after the first 4–5 days.

The stress-strain curves for pristine and soaked solid polydomain LCEs loaded in tension are plotted in Fig. 7b. After 21 days of soaking, the overall tensile response of the soaked material compared to the pristine condition was not substantially different. However, the critical stress to initiate the soft-elastic effect slightly decreased from approximately 65 kPa for pristine samples, down to 56 kPa for soaked samples.

The creep response for the pristine and soaked solid polydomain LCEs was studied at two stress levels: 100 kPa and 25 kPa. These stresses correlate to values above and below the soft-elastic initiation stress, respectively, observed in tensile testing at 1%/s strain rate. The purpose of this scheme is to investigate the creep response with and without the influence of mesogen rotation in response to the applied stress. The first 15 s of the creep strain as a function of time is plotted for both samples and stress levels in Fig. 7c. In all cases, the strain increased rapidly before reaching a steady-state value within the first 5 s of the test. At the 25 kPa stress level, the creep behavior was virtually unchanged between the pristine and soaked samples. At the 100 kPa stress level, the soaked sample reached a slightly lower equilibrium strain. The pristine sample reached 85% strain while the soaked sample only reached 82% strain. For reference, during the quasi-static tensile test, 87% strain was measured at 100 kPa. Although the 100 kPa creep stress level was above the soft elasticity initiation stress, no observable deviation from a typical creep response stemmed from the mesogen alignment phenomenon.

3.4. In-vivo biocompatibility

The subcutaneous physiological response of solid and porous polydomain LCE materials was studied by *in vivo* implantation in rats. Representative images of the implants upon removal and staining are found in Fig. 8. The H&E staining was used to study tissue infiltration, cellularity and structure into the pores and surrounding the material implants (Fig. 8a). Hematoxylin stained the nuclei of cells blue while the Eosin stained the extracellular matrix and the cell cytoplasm pink. Masson's Trichrome staining was used to stain for fibrotic tissue around the material implant, with cytoplasm staining red, collagen staining blue, and nuclei black (Fig. 8b). The porous implant was surrounded on average by a 340 μm thick layer of fibrous tissue. Ingrowth of tissue into the porous structure of the scaffold was observed at an average depth of 820 μm into the sample. In contrast, the solid implants had a much thinner layer of fibrotic encapsulation with an average thickness of 80 μm ; no tissue ingrowth could be observed. Neither the solid nor porous samples showed any obvious inflammatory response or noticeable swelling on the animal.

3.5. Proof of concept total disc replacement device

The properties of the LCE materials were compared to human intervertebral disc tissue (Fig. 9a). Both the annulus fibrosus and the nucleus pulposus exhibited behavior similar to a conventional elastomer and could be reasonably modeled by an exponentially increasing curve. At strains under 15%, the response is nearly identical. However, modulus of the annulus fibrosus increases rapidly with further deformation. When compared to the nucleus pulposus, the solid polydomain material exhibits strikingly similar compressive behavior, only diverging slightly at large deformations. The monodomain material loaded longitudinally also exhibits a compressive response similar to the

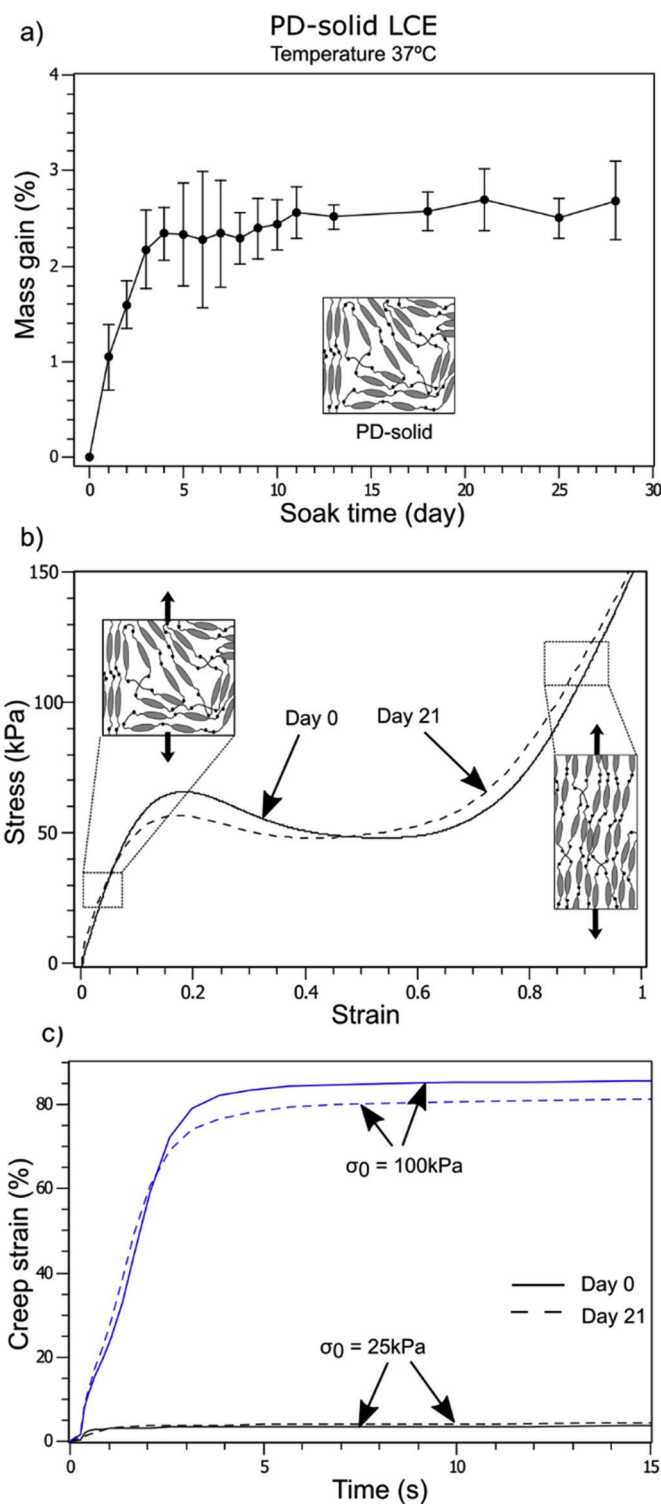


Fig. 7. (a) Mass gain as a function of soaking duration in phosphate buffer saline solution for solid polydomain LCE samples. The mass gain reached an equilibrium of approximately 2.5 wt.% within approximately five days. (b) Representative tensile response of as-fabricated solid polydomain LCE and solid polydomain LCE soaked for 21 days. The samples were tested at 37 °C and a strain rate of 1%/s. Solid polydomain LCE demonstrated similar mechanical behavior after soaking compared to the pristine condition. (c) Tensile creep tests of the as-fabricated and soaked solid polydomain LCE showed a nearly identical response. The selected creep stress levels were just below and just above the critical stress required to initiate soft elasticity. The tests were run at 37 °C.

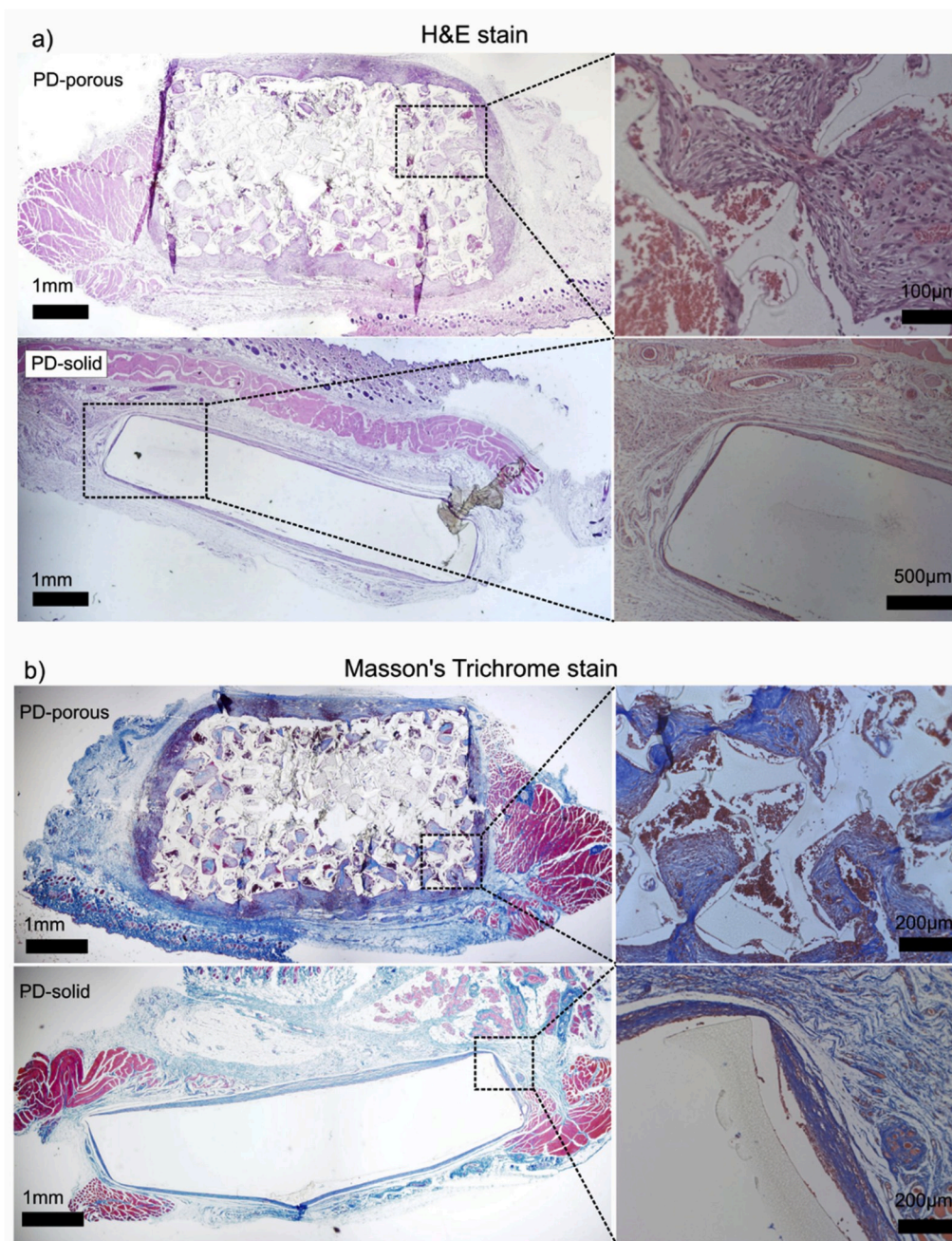
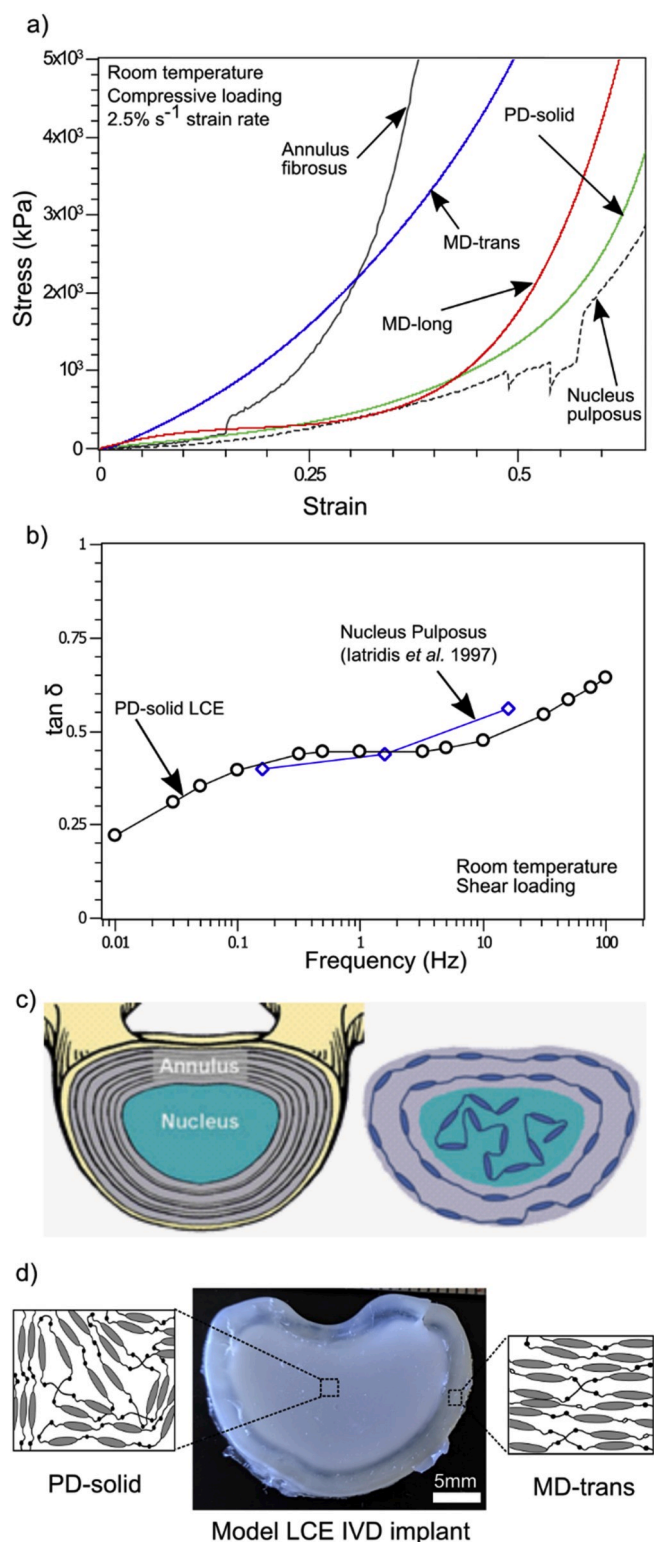


Fig. 8. Histology assessment of solid and porous polydomain LCEs after sub-cutaneous implantation in Sprague Dawley rats. The semi-circular disc solid and porous polydomain LCE samples were implanted for four weeks and then assessed using (a) H&E staining, and (b) Masson's trichrome staining upon removal. The images showed fibrotic encapsulation around both the solid and porous polydomain LCE samples, and tissue infiltration into the voids of the porous polydomain LCE samples.

nucleus pulposus. Up to moderate strains, the soft-elastic plateau closely matches the stress-strain plot of the nucleus pulposus, but the modulus of the monodomain material increased at larger deformations. When compared to the annulus fibrosus, none of these LCE materials demonstrate identical behavior. However, the monodomain material loaded transversely showed reasonably similar response up to moderate strains of approximately 40%.

Iatridis et al. had previously studied the damping behavior of the nucleus pulposus using a dynamic shear frequency sweep test and reported the damping parameter $\tan \delta$ as a function of frequency (Iatridis et al., 1997b). Similar experimental data for solid polydomain LCEs was obtained and plotted against the literature data, as shown in Fig. 9b. In both cases, the damping parameter increases with frequency over the testing range. Furthermore, the damping behavior of polydomain LCE material is similar to the nucleus pulposus in both magnitude and apparent trend, at least over the limited literature data available.

Ultimately, a proof of concept artificial intervertebral disc was fabricated to mimic collagen alignment in IVD with mesogen alignment (Fig. 9c). The prototype (Fig. 9d) was constructed using solid monodomain material with transversely aligned mesogens around the exterior, as a substitute for the annulus fibrosus; and solid polydomain material in the center, as a substitute for the nucleus pulposus. This configuration was selected as it most closely mimics the structure and mechanical behavior of an actual intervertebral disc based on the compressive and dynamic shear testing performed. The device was fabricated by first casting the monodomain LCE forming material into an annulus fibrosus-shaped mold with scaled-down perimeter and scaled-up cross-section. This molded part was subsequently stretched and cured using ultraviolet polymerization to lock the alignment, and the annulus fibrosus-shaped monodomain LCE was achieved. Finally, the polydomain LCE forming material was poured inside the monodomain LCE annulus fibrosus structure and allowed to cure in the nematic phase



(caption on next column)

Fig. 9. (a) Representative curves for monotonic compression of the annulus fibrosus and nucleus pulposus of a cadaver intervertebral disc compared to solid polydomain, and longitudinally and transversely loaded monodomain LCE materials. The solid polydomain, and longitudinally loaded monodomain LCE materials demonstrated roughly similar behavior to the nucleus pulposus. The transversely loaded monodomain LCE material was closest to the annulus fibrosus. All the samples were tested in ambient conditions at a strain rate of $2.5\%/s$. (b) The plot of the damping parameter $\tan \delta$ vs. frequency for the nucleus pulposus and solid polydomain LCE. The damping capacities are similar over a broad range of frequencies. The data for the nucleus pulposus was obtained from the literature (latridis et al., 1997b). The solid polydomain LCE sample was tested in shear loading at ambient conditions similar to the literature. (c) A schematic diagram shows model IVD is devised by mimicking the collagen alignment with the LCE's mesogen alignment. (d) The model IVD implant made from LCE materials. Solid polydomain LCE was selected as an analog for the nucleus pulposus while transversely aligned monodomain material was selected as an analog for the annulus fibrosus. The outer transversely aligned monodomain surrounded the central polydomain region.

to create a polydomain LCE nucleus pulposus. This simple proof of concept implant demonstrates the ability to utilize the anisotropic behavior of LCEs to more closely match complex biological structures.

4. Discussion

4.1. Synthesis methods

There are slight differences between the polydomain and monodomain samples beyond simply the global mesogen alignment. Polydomain materials were allowed to cool at ambient temperatures while network forming Michael Addition reaction was occurring. At room temperature, the polymer network formed when the mesogens were in a nematic alignment; this is termed nematic genesis (Traugutt et al., 2017). Conversely, the monodomain materials were completely cured at an elevated temperature and then allowed to cool to ambient conditions, followed by subsequent stretching and photopolymerization. The elevated temperature during curing was above the isotropic transition temperature meaning that no localized order was present during network formation; this is termed isotropic genesis (Saed et al., 2017; Traugutt et al., 2017). Ultimately, when the cured network is allowed to cool, it will still result in a nematic polydomain conformation, but the domains of alignment will be much smaller than those obtained using a nematic genesis technique. The isotropic genesis scheme was selected when fabricating monodomain materials because the smaller domains rotate more efficiently and with less applied force. During stretching and photopolymerization, this ensures that the maximum alignment of the mesogens is achieved. Since the smaller domains tend to align more easily, this also maximizes the soft-elastic effect and ensures that the monodomain materials manifest strongly anisotropic behavior.

4.2. Mechanical behavior

Solid polydomain, solid monodomain, and porous polydomain LCE materials were all tested in uniaxial tension and compression, and each class exhibited unique mechanical properties. Polydomain samples tested in tension, monodomain samples transversely loaded in tension, and monodomain samples longitudinally loaded in compression all exhibited soft elasticity. This soft elasticity is a result of mesogen rotation and alignment and results in a large stress plateau region. The mesogen rotation is a largely hysteretic effect and gives LCEs exceptional energy dissipation over a wide range of temperatures and frequencies. Closely related, the large stress plateau also makes LCEs highly efficient at absorbing energy from impulse loading. Interestingly, the mechanical response of the solid monodomain LCE loaded longitudinally in compression is not unlike that of traditional foam. The effect of soft elasticity is mirrored by cell collapse and eventual densification in

conventional porous materials, resulting in similar stress plateaus of the corresponding stress-strain curves. However, this LCE is a solid material rather than a foam, and thus has greater stiffness, strength, elasticity and energy absorption capacity to conventional porous polymers. This desirable combination of properties makes LCEs uniquely suited for many load-bearing biomedical applications.

Not all classes of LCEs nor loading scenarios will result in the soft-elastic effect. The effect is most prominent when maximum mesogen rotation is present. Monodomain solid LCEs loaded transversely in tension allow the most dramatic change in director alignment, and by virtue yields the largest magnitude soft elasticity; the stress is nearly constant between 10-110% strain. Logically, polydomain solid LCEs have no ordered global alignment, and thus less mesogen rotation is required when pulled in tension. The soft-elastic effect is still present and readily apparent but will reach complete alignment earlier than the transversely loaded monodomain samples, ranging from about 15-70% strain. Monodomain solid LCEs loaded longitudinally in compression still exhibit a soft-elastic effect, but it is greatly diminished. The reasons for this are two-fold. First, in compression, the mesogens align with the plane perpendicular to the loading direction, creating a negative order parameter (Jampani et al., 2019). This plane has greater geometric freedom in terms of mesogen alignment compared to a single line or direction when loaded in tension. Ultimately, less mesogen rotation is required to align with the plane, and as a result, the soft-elastic effect will occur over a smaller deformation. Second, the material deforms fast and the cross-sectional area increases rapidly during the compressive loading, simulating a densification similar phenomenon. The material keeps stiffening as it is compressed, and the stress required for further deformation increases exponentially. The stiffening behavior effectively suppresses the soft-elastic effect. Lastly, it also can be observed that the critical stress before initiation of the soft-elastic plateau is lower for the monodomain material loaded longitudinally in compression than the monodomain material loaded transversely in tension. It is theorized that this lower critical stress is a result again of alignment towards a plane rather than a single direction. After only a small amount of mesogen rotation, more progress has likely been made towards alignment with the plane in compression, compared to an equivalent amount of progress that could have been achieved with alignment to a single direction during tensile loading. The result is that bulk director rotation occurs sooner in compression and completes faster.

In certain combinations of mesogen configuration and loading direction, the soft-elastic effect is not present at all. The most obvious example is the monodomain material longitudinally loaded in tension and transversely loaded in compression. In these cases, the mesogens are already aligned with the loading direction for tension and the plane perpendicular to the loading direction for compression. Since no director rotation occurs, the samples behave in a linear elastic manner with a slightly higher modulus in compression than in tension. Polydomain LCEs in compression exhibit no soft elasticity, for the same reasons that it is suppressed in the monodomain material longitudinally loaded in compression. Since there is no initial global alignment in the polydomain LCEs, any soft elasticity is completely shadowed by the easier alignment to a plane and the rapid increase in the cross-sectional area. Porous LCEs demonstrate no soft-elastic effect in either tension or compression. The size of the pores is much greater than the local domains of alignment, and the pores are randomly distributed and aligned. Instead of mesogen alignment or rotation, the dominant behavior is bending and buckling of the cell walls. The resulting mechanical response is emblematic of traditional porous materials.

4.3. Exposure to physiological condition

Water contact angle testing indicated that all LCE samples were slightly hydrophilic, with contact angles below 90° (Kulkarni and Shaw, 2016; Laursen et al., 2016). It is theorized that the water contact angle is largely dependent on the material composition. The solid and porous

polydomain materials exhibited very similar contact angles, while the monodomain material had a slightly higher angle, potentially due to the larger acrylate content. Reflective of their hydrophilic nature, the tested solid polydomain sample absorbed a limited amount of water within the first few days of soaking in a phosphate buffer saline solution. The absorbed water content for the solid polydomain LCE stabilized after one week of soaking at approximately 2.5% by mass. While this amount of absorbed water mass gain is typical for similar polymers (Lakhera et al., 2012; Smith et al., 2009), LCEs with hydrophilicity high enough to form hydrogels have been reported (Torbati and Mather, 2016).

In order to study the effects of water mass gain on the mechanical behavior of LCEs, uniaxial tension and creep tests were performed on solid polydomain LCE samples before and after soaking. In brief, the mechanical responses for both tests are relatively stable, and deviations from the pristine behavior were minimal. It has been reported in previous literature that absorbed water can act as a plasticizer (Smith et al., 2009), and that absorbed water can additionally disrupt the mesogen order (Torbati and Mather, 2016). Absorbed water acting as a plasticizer could cause lower soft-elastic initiation stress, as well as the lower equilibrium creep strain, as was observed for the soaked materials. However, there is no evidence that the liquid crystalline order was disrupted by absorbed water for the soaked LCEs presented here.

4.4. In-vivo biocompatibility

Before any use of LCEs as a biomedically relevant material can be justified, an investigation into the various aspects of biological compatibility must be pursued. Previous work has demonstrated that LCEs of a similar composition to those used in this study have no cytotoxic effect (Yakacki et al., 2015). A more rigorous measure of compatibility is *in vivo* subcutaneous implantation, which was studied for solid and porous LCEs in rats, as shown in Fig. 8. Subsequent staining revealed fibrous encapsulation around the solid material and tissue integration into the porous material. No adverse conditions were observed as a result of implantation and all rats were considered healthy throughout the trial period. It is known that the hydrophilicity of material usually promotes biocompatibility (Hezi-yamit et al., 2009; Oh and Lee, 2013). Therefore, the moderate hydrophilicity observed in the LCEs here has helped their positive biocompatibility.

To reduce the possibility of a harmful biological reaction, porous LCEs were fabricated using a simple salt leaching technique (Loh and Choong, 2013). This methodology makes the use of harsh organic solvents unnecessary and reduces the risk of residual toxic elements. For the trabecular bone and the vertebral endplate, typically, the porosity is in the range of 40–90% (Karageorgiou and Kaplan, 2005; Rodriguez et al., 2012) and the pore size is in the order of 100–900 μm (Hildebrand et al., 1999; Rodriguez et al., 2012). In various bone and cartilage regeneration scaffolds and interbody fusion devices, 50–90% porosity and 100–600 μm pores have been utilized (Al-Munajjed et al., 2008; Karageorgiou and Kaplan, 2005; Torstrick et al., 2017). Therefore, to develop material to be used in a similar biological environment, the porous LCE with approximately 54% porosity and 250–420 μm pore sizes was aimed in this study. To reach the target porosity range, a 1:2 wt ratio of salt to LCE was chosen. Approximating the density of the salt being approximately twice of the LCEs, the LCE was expected to yield approximately 50% porosity, which is in the fair agreement of the measured porosity of 54%. Furthermore, the pore size and structure can be easily modified utilizing different sized or shaped salt crystals to enhance or suppress cellular integration, if desired. As the mechanical properties of a specific porous material are function of the pore geometry (i.e. open-cell vs. closed-cells) and the density ratio of the porous to solid material (Gibson and Ashby, 1982; Sun et al., 2016), any change to pore size and structure is not expected to impact the mechanical properties of the LCEs significantly, when the pore volume fraction is kept constant. However, the higher porosity would have led to much lower stiffness, but possibly would allow more tissue ingrowth during the *in*

in vivo study as well (Murphy et al., 2010). Despite the very promising result of tissue ingrowth into the porous LCEs, very low stiffness, compared to the solid polydomain as observed in Fig. 5, made it potentially unsuitable for this specific load-bearing application described in this paper. Nevertheless, the porous LCE has potential for biomedical devices where less load-bearing capacity is required, such as neuronal tissue scaffold (Mori et al., 2020), artificial skin (Sharma et al., 2017), porous surface of higher strength interbody fusion cage (Torstrick et al., 2017) etc.

The stable mechanical behavior in physiological conditions, non-cytotoxic response, and inert behavior during subcutaneous implantation are all strong evidence towards validating the biological compatibility of LCEs. Of course, much work remains to be realized, and the material must undergo additional study, screening, and clinical evaluation before it could be considered for use as a load-bearing biomedical material.

4.5. Proof of concept TDR device

A proof of concept total disc replacement device was constructed using two classes of LCE materials designed to better mimic biological structure and function. Uniaxial compressive testing revealed that monodomain LCE loaded transversely has a similar mechanical response to the annulus fibrosus (Fig. 9a). In application, relevant average loads on the intervertebral discs can be estimated as 1.2 times bodyweight (O'Connell et al., 2011). This magnitude of stress should not exceed 15% strain of the intervertebral discs (O'Connell et al., 2011). More importantly, transversely loaded monodomain LCEs do not undergo soft elasticity during deformation. Since there is no bulk rotation or realignment of the mesogens, the material recovers much faster when the applied load is removed. Although this increased elasticity comes at the expense of the mechanical damping and energy dissipation characteristics. The role of the annulus fibrosus is to provide structure, elasticity, and support for the nucleus pulposus, and the disc as a whole. For these reasons, transversely aligned monodomain LCE material was selected as an analog for the annulus fibrosus.

The role of the nucleus pulposus is to provide mechanical damping for the intervertebral disc and has been found to be highly viscoelastic (Iatridis et al., 1996). Of the materials tested in compression, the samples with the closest mechanical response were the solid polydomain material and the longitudinally loaded monodomain material. Due to its soft-elastic behavior, the monodomain LCE possesses extremely high damping properties but prolonged recovery and quasi-permanent deformation, because it is difficult for the mesogens to return to the original aligned configuration without heat or a mechanical bias. The solid polydomain material tested here exhibits a nearly identical compressive response to the nucleus pulposus over the region of interest, as well as, very similar shear damping behavior in terms of magnitude and trend relative to frequency. Furthermore, our previous study of the polydomain LCE with the same composition demonstrated strong loss tangent over a broad range of temperatures under small amplitude oscillating strain (Merkel et al., 2019). The polydomain LCE material also showed high energy dissipation and fast strain recovery when tested under large-amplitude cyclic loading at a temperature close to the human body temperature (Merkel et al., 2019). Thus, polydomain LCE material was a natural candidate to perform energy dissipation functionality and selected as the analog for the nucleus pulposus.

The capability of LCEs to mimic the very diverse behavior demonstrated by annulus fibrosus and nucleus pulposus can be attributed to the presence of its unique soft elasticity. The soft elastic response of LCE facilitates its superior energy dissipation capacity (Merkel et al., 2019). The inherent soft elasticity of the solid polydomain LCE allowed it to match the large $\tan \delta$ over a broad range of frequency demonstrated by the nucleus pulposus. Furthermore, the underlying mechanism for the soft elasticity is the mesogen rotation, which in turn allows achieving the monodomain material with highly anisotropic mechanical behavior.

Subsequently, it was possible for LCEs with the same chemistry to match the mechanical behavior of different segments of the intervertebral disc. Conventional elastomers, i.e., non-LCEs, can possibly be designed by varying chemical composition and crosslink density to match just the stress-strain behavior of the nucleus pulposus and annulus fibrosus. However, the lack of the soft elastic behavior of the non-LCEs will limit their energy dissipation capacity and consequently, they will be unable to mimic the large magnitude of $\tan \delta$ of nucleus pulposus over broad the frequency range.

The simple device was fabricated with transversely aligned monodomain LCEs around the exterior with polydomain LCEs cast into the center. The desire is that the combined properties of the two classes of LCEs will more accurately mimic actual biological function. Although the testing of the current device is ongoing, the results demonstrated thus far warrant a much deeper effort and an iterative design methodology will be implemented moving forward. By optimizing other parameters such as crosslink density, the functionality and type of monomers utilized, structured geometries, and the amount of excess acrylate, it should be possible to narrow in on an optimal design (Merkel et al., 2018; Saed et al., 2017). While the focus has been on an intervertebral disc, the scope of applications should not be confined to this one device. For example, we have also recently explored the use of dynamically-crystallizing LCEs that can be 3D-printed to serve as a spinal fusion cage (Volpe et al., 2019). The unique variety of properties LCEs possess, and their tailorable nature could make the material an excellent choice for load-bearing biomedical applications including the replacement of complex cartilaginous tissues of the joints.

5. Conclusions and outlook

The driving intent of this work was to evaluate the candidacy of LCEs materials as a suitable choice in load-bearing biomedical applications. Three classes of LCEs with similar compositions but different mechanical behaviors were studied: solid polydomain, porous polydomain, and solid monodomain. The investigation was guided by three objectives. First, what are the mechanical responses and potential anisotropy for each class of material. Second, how is the mechanical response of each material affected by physiological conditions and *in vivo* subcutaneous implantation. Lastly, how can the diverse properties of LCEs be utilized to more closely mimic the biological function in a proof of concept total disc replacement device.

Due to the integration of a liquid crystalline mesogen backbone, the mechanical properties of LCEs can be both unique and varied. The solid polydomain material exhibits moderate soft elasticity when pulled in tension, while the compressive response is more characteristic of a traditional polymer. The porous LCEs are logically much softer than the solid material, but the soft-elastic effect was not present under either tension or compression load. Instead, the macroscopic porous structure made buckling and collapse of the cell walls the dominant deformation mechanism. The monodomain materials exhibited a truly anisotropic mechanical response with different behavior in tension and compression. The monodomain material loaded transversely in tension and longitudinally in compression both demonstrated soft elasticity, owing to their mesogen rotation in response to the load. Since nearly no mesogen rotation is required, transversely loaded material in compression, and longitudinally loaded material in tension displayed only linear elastic behavior. Depending on the mesogen orientations and loading conditions, the LCEs span a range of mechanical properties from high elasticity with rapid recovery, to highly viscoelastic with a strong hysteretic nature.

As part of the investigation on how LCEs will react in the biological environment, the water contact angle testing revealed that all classes of LCEs are slightly hydrophilic. After two weeks of soaking in a phosphate buffer saline solution, the solid polydomain LCEs absorbed approximately 2.5% weight percent water. However, creep and tensile testing revealed that this absorbed water has only a limited effect on

mechanical properties. Specifically, the equilibrium creep strain and the soft-elastic initiation stress both decreased marginally. Subcutaneous implantation in rats revealed fibrous encapsulation around solid polydomain materials and cellular integration in porous materials. Additionally, no swelling or inflammatory response was observed, and no other adverse medical conditions were recognized during the implantation period. Paired with previous reports that demonstrated *in vitro* non-cytotoxicity, these findings are strong evidence towards verifying LCEs as a safe and stable material for use in physiological conditions and fulfilling applications as a biomaterial. Naturally, testing such as hemocompatibility, pyrogenicity, carcinogenicity, and clinical evaluation remains to be performed before a full biological compatibility assessment can be completed.

In fulfillment of the last objective proposed for this work, a proof of concept total disc replacement device was fabricated. The simple prototype incorporated two different configurations of LCEs designed to independently simulate the behavior of the annulus fibrosus and the nucleus pulposus. The strong elasticity and rigid structure of transversely aligned monodomain material led its selection as an analog for the annulus fibrosus, while the high damping characteristics and moderate stiffness of polydomain material led to its selection as an analog for the nucleus pulposus. This combination of properties is intended to more closely match the actual response of a human intervertebral disc. Moreover, the wide range of available mechanical properties, soft-elastic effect, and strong anisotropy give LCEs highly customizable behavior. It is evident that these unique attributes make LCEs well suited for load-bearing biomedical applications.

Funding sources

Funding support from the NSF-CAREER grant (Grant No. CMMI-1350436) and the NSF-PFI grant (Grant No. 1827288) is gratefully acknowledged.

Declaration of competing interest

CPF, CMY and AHT have financial interest in Impressio Inc. – a company involved in the development of biomedical and engineering products based on the Liquid Crystalline Elastomers. Authors have no other interest to declare.

Acknowledgments

The authors would like to thank Mansoureh Norouzi Rad of Carl Zeiss Microscopy, LLC for their help with X-ray microscopy images.

References

- Al-Munajjed, A.A., Hien, M., Kujat, R., Gleason, J.P., Hammer, J., 2008. Influence of pore size on tensile strength, permeability and porosity of hyaluronan-collagen scaffolds. *J. Mater. Sci. Mater. Med.* 19, 2859–2864. <https://doi.org/10.1007/s10856-008-3422-5>.
- Avalle, M., Belingardi, G., Montanini, R., 2001. Characterization of polymeric structural foams under compressive impact loading by means of energy-absorption diagram. *Int. J. Impact Eng.* 25, 455–472. [https://doi.org/10.1016/S0734-743X\(00\)00060-9](https://doi.org/10.1016/S0734-743X(00)00060-9).
- Azoug, A., Vasconcellos, V., Dooling, J., Saed, M., Yakacki, C.M., Nguyen, T.D., 2016. Viscoelasticity of the polydomain-monodomain transition in main-chain liquid crystal elastomers. *Polymer* 98, 165–171. <https://doi.org/10.1016/j.polymer.2016.06.022>.
- Bera, T., Freeman, E.J., McDonough, J.A., Clements, R.J., Aladlaan, A., Miller, D.W., Malcuit, C., Hegmann, T., Hegmann, E., 2015. Liquid crystal elastomer microspheres as three-dimensional cell scaffolds supporting the attachment and proliferation of myoblasts. *ACS Appl. Mater. Interfaces* 7, 14528–14535. <https://doi.org/10.1021/acsami.5b04208>.
- Beyer, P., Terentjev, E.M., Zentel, R., 2007. Monodomain liquid crystal main chain elastomers by photocrosslinking. *Macromol. Rapid Commun.* 28, 1485–1490. <https://doi.org/10.1002/marc.200700210>.
- Boothby, J.M., Kim, H., Ware, T.H., 2017. Shape changes in chemoresponsive liquid crystal elastomers. *Sensor. Actuator. B Chem.* 240, 511–518. <https://doi.org/10.1016/j.snb.2016.09.004>.
- Brannum, M.T., Steele, A.M., Venetos, M.C., Korley, L.S.T.J., Wnek, G.E., White, T.J., 2019. Light control with liquid crystalline elastomers. *Adv. Opt. Mater.* 1801683, 1–7. <https://doi.org/10.1002/adom.201801683>.
- Buguin, A., Li, M.H., Silberzan, P., Ladoux, B., Keller, P., 2006. Micro-actuators: when artificial muscles made of nematic liquid crystal elastomers meet soft lithography. *J. Am. Chem. Soc.* 128, 1088–1089. <https://doi.org/10.1021/ja0575070>.
- Chrastil, J., Patel, A.A., 2012. Complications associated with posterior and transforaminal lumbar interbody fusion. *J. Am. Acad. Orthop. Surg.* 20, 283–291. <https://doi.org/10.5435/JAAOS-20-05-283>.
- Clarke, S.M., Tajbakhsh, A.R., Terentjev, E.M., Remillat, C., Tomlinson, G.R., House, J.R., 2001. Soft elasticity and mechanical damping in liquid crystalline elastomers. *J. Appl. Phys.* 89, 6530–6535. <https://doi.org/10.1063/1.1368177>.
- Cortes, D.H., Elliott, D.M., 2014. The intervertebral disc: overview of disc mechanics. In: Shapiro, I.M., Risbud, M.V. (Eds.), *The Intervertebral Disc: Molecular and Structural Studies of the Disc in Health and Disease*. Springer Vienna, Vienna, pp. 17–31. https://doi.org/10.1007/978-3-7091-1535-0_2.
- De Gennes, P.-G., Hébert, M., Kant, R., 1997. Artificial muscles based on nematic gels. *Macromol. Symp.* 113, 39–49. <https://doi.org/10.1002/masy.19971130107>.
- Donald, A., Windle, A., Hanna, S., 2006. *Liquid Crystalline Polymers*, second ed. Cambridge University Press, pp. 1–589. <https://doi.org/10.1017/CBO9780511616044>.
- Ferrantini, C., Pioner, J.M., Martella, D., Coppini, R., Piroddi, N., Paoli, P., Calamai, M., Pavone, F.S., Wiersma, D.S., Tesi, C., Cerbai, E., Poggesi, C., Sacconi, L., Parmeggiani, C., 2019. Development of light-responsive liquid crystalline elastomers to assist cardiac contraction. *Circ. Res.* 124. <https://doi.org/10.1161/CIRCRESAHA.118.313889> e44–e54.
- Finkelmann, H., Kock, H.-J., Rehage, G., 1981. Investigations on liquid crystalline polysiloxanes 3. Liquid crystalline elastomers—a new type of liquid crystalline material. *Makromol. Chem., Rapid Commun.* 2, 317–322. <https://doi.org/10.1002/marc.1981.030020413>.
- Gao, Y., Mori, T., Manning, S., Zhao, Y., Nielsen, A.D., Neshat, A., Sharma, A., Mahnen, C.J., Everson, H.R., Crotty, S., Clements, R.J., Malcuit, C., Hegmann, E., 2016. Biocompatible 3D liquid crystal elastomer cell scaffolds and foams with primary and secondary porous architecture. *ACS Macro Lett.* 5, 4–9. <https://doi.org/10.1021/acsmacrolett.5b00729>.
- Ge, F., Zhao, Y., 2019. Microstructured actuation of liquid crystal polymer networks. *Adv. Funct. Mater.* 1901890, 1901890. <https://doi.org/10.1002/adfm.201901890>.
- Gibson, L.J., Ashby, M.F., 1982. The mechanics of three-dimensional cellular materials. *Proc. R. Soc. A Math. Phys. Eng. Sci.* 382, 43–59. <https://doi.org/10.1098/rspa.1982.0088>.
- Hezi-yamit, A., Sullivan, C., Wong, J., David, L., Chen, M., Cheng, P., Shumaker, D., Wilcox, J.N., Udipti, K., Cardiovascular, M., Rosa, S., 2009. Impact of polymer hydrophilicity on biocompatibility: implication for DES polymer design. *J. Biomed. Mater. Res. Part A* 90A 133–141. <https://doi.org/10.1002/jbm.a.32057>.
- Hildebrand, T., Laib, A., Müller, R., Dequeker, J., Rügsegger, P., 1999. Direct three-dimensional morphometric analysis of human cancellous bone: microstructural data from spine, femur, iliac crest, and calcaneus. *J. Bone Miner. Res.* 14, 1167–1174. <https://doi.org/10.1359/jbmr.1999.14.7.1167>.
- Hiraoka, K., Tagawa, N., Baba, K., 2008. Shape-memory effect controlled by the crosslinking topology in uniaxially-deformed smectic C elastomers. *Macromol. Chem. Phys.* 209, 298–307. <https://doi.org/10.1002/macp.200700387>.
- Huang, R.C., Tropiano, P., Marnay, T., Girardi, F.P., Lim, M.R., Cammisia, F.P., 2006. Range of motion and adjacent level degeneration after lumbar total disc replacement. *Spine J.* 6, 242–247. <https://doi.org/10.1016/j.spinee.2005.04.013>.
- Hyde, P.J., Fisher, J., Hall, R.M., 2017. Wear characteristics of an unconstrained lumbar total disc replacement under a range of *in vitro* test conditions. *J. Biomed. Mater. Res. B Appl. Biomater.* 105, 46–52. <https://doi.org/10.1002/jbm.b.33456>.
- Iatridis, J.C., Setton, L.A., Weidenbaum, M., Mow, V.C., 1997a. The viscoelastic behavior of the non-degenerate human lumbar nucleus pulposus in shear. *J. Biomech.* 30, 1005–1013. [https://doi.org/10.1016/S0021-9290\(97\)00069-9](https://doi.org/10.1016/S0021-9290(97)00069-9).
- Iatridis, J.C., Setton, L.A., Weidenbaum, M., Mow, V.C., 1997b. Alterations in the mechanical behavior of the human lumbar nucleus pulposus with degeneration and aging. *J. Orthop. Res.* 15, 318–322. <https://doi.org/10.1002/jor.1100150224>.
- Iatridis, J.C., Weidenbaum, M., Setton, L.A., Mow, V.C., 1996. Is the nucleus pulposus a solid or a fluid? Mechanical behaviors of the nucleus pulposus of the human intervertebral disc. *Spine* 21, 1174–1184. <https://doi.org/10.1097/00007632-199605150-00009>. Phila. Pa. 1976.
- Ikeda, T., Mamiya, J.I., Yu, Y., 2007. Photomechanics of liquid-crystalline elastomers and other polymers. *Angew. Chem. Int. Ed.* 46, 506–528. <https://doi.org/10.1002/anie.200602372>.
- Inoue, Y., Atsumi, Y., Kawamura, A., Miyata, T., 2019. Thermoresponsive liquid crystalline polymer membranes that undergo phase transition at body temperature. *J. Membr. Sci.* 588, 117213. <https://doi.org/10.1016/j.memsci.2019.117213>.
- Jampani, V.S.R., Volpe, R.H., Reguengo de Sousa, K., Ferreira Machado, J., Yakacki, C.M., Lagerwall, J.P.F., 2019. Liquid crystal elastomer shell actuators with negative order parameter. *Sci. Adv.* 5, eaaw2476. <https://doi.org/10.1126/sciadv.aaw2476>.
- Karageorgiou, V., Kaplan, D., 2005. Porosity of 3D biomaterial scaffolds and osteogenesis. *Biomaterials* 26, 5474–5491. <https://doi.org/10.1016/j.biomaterials.2005.02.002>.
- Katz, J.N., 2006. Lumbar disc disorders and low-back pain: socioeconomic factors and consequences. *J. Bone Joint Surg. Am.* 88 (Suppl. 2), 21–24. <https://doi.org/10.2106/JBJS.E.01273>.
- Kim, H.J., Kelly, M.P., Ely, C.G., Riew, K.D., Dettori, J.R., 2012. The risk of adjacent-level ossification development after surgery in the cervical spine: are there factors that affect the risk? A systematic review. *Spine* 37, 65–74. <https://doi.org/10.1097/BRS.0b013e31826cb8f5>. Phila. Pa. 1976.

- Kularatne, R.S., Kim, H., Boothby, J.M., Ware, T.H., 2017. Liquid crystal elastomer actuators: synthesis, alignment, and applications. *J. Polym. Sci., Part B: Polym. Phys.* 55, 395–411. <https://doi.org/10.1002/polb.24287>.
- Kulkarni, V.S., Shaw, C., 2016. Surfactants, lipids, and surface chemistry. In: *Essential Chemistry for Formulators of Semisolid and Liquid Dosages*. Elsevier, pp. 5–19. <https://doi.org/10.1016/B978-0-12-801024-2.00002-9>.
- Lakhera, N., Smith, K.E., Frick, C.P., 2012. Systematic tailoring of water absorption in photopolymerizable (meth)acrylate networks and its effect on mechanical properties. *J. Appl. Polym. Sci.* <https://doi.org/10.1002/app.38371> n/a-n/a.
- Laursen, C.M., Brant, J.A., Frick, C.P., 2016. A methodology for fabrication of thermomechanically activated switchable surface wettability. *J. Appl. Polym. Sci.* 133, 1–14. <https://doi.org/10.1002/app.44122>.
- Li, C., Liu, Y., Huang, X., Jiang, H., 2012. Direct sun-driven artificial heliotropism for solar energy harvesting based on a photo-thermomechanical liquid-crystal elastomer nanocomposite. *Adv. Funct. Mater.* 22, 5166–5174. <https://doi.org/10.1002/adfm.201202038>.
- Li, M.-H., Keller, P., 2006. Artificial muscles based on liquid crystal elastomers. *Philos. Trans. R. Soc. A Math. Phys. Eng. Sci.* 364, 2763–2777. <https://doi.org/10.1098/rsta.2006.1853>.
- Loh, Q.L., Choong, C., 2013. Three-dimensional scaffolds for tissue engineering applications: role of porosity and pore size. *Tissue Eng. B Rev.* 19, 485–502. <https://doi.org/10.1089/ten.teb.2012.0437>.
- Martella, D., Parmeggiani, C., 2018. Advances in cell scaffolds for tissue engineering: the value of liquid crystalline elastomers. *Chem. Eur. J.* 24, 12206–12220. <https://doi.org/10.1002/chem.201800477>.
- Merkel, D.R., Shaha, R.K., Yakacki, C.M., Frick, C.P., 2019. Mechanical energy dissipation in polydomain nematic liquid crystal elastomers in response to oscillating loading. *Polymer* 166, 148–154. <https://doi.org/10.1016/j.polymer.2019.01.042>.
- Merkel, D.R., Traugott, N.A., Visvanathan, R., Yakacki, C.M., Frick, C.P., 2018. Thermomechanical properties of monodomain nematic main-chain liquid crystal elastomers. *Soft Matter* 14, 6024–6036. <https://doi.org/10.1039/C8SM01178H>.
- Mori, T., Cukelj, R., Prévôt, M.E., Ustunel, S., Story, A., Gao, Y., Diabre, K., McDonough, J.A., Freeman, E.J., Hegmann, E., Clements, R.J., 2020. 3D porous liquid crystal elastomer foams supporting long-term neuronal cultures. *Macromol. Rapid Commun.* 1900585, 1900585. <https://doi.org/10.1002/marc.201900585>.
- Murphy, C.M., Haugh, M.G., O'Brien, F.J., 2010. The effect of mean pore size on cell attachment, proliferation and migration in collagen-glycosaminoglycan scaffolds for bone tissue engineering. *Biomaterials* 31, 461–466. <https://doi.org/10.1016/j.biomaterials.2009.09.063>.
- Nagahama, K., Ueda, Y., Ouchi, T., Ohya, Y., 2007. Exhibition of soft and tenacious characteristics based on liquid crystal formation by introduction of cholesterol groups on biodegradable lactide copolymer. *Biomacromolecules* 8, 3938–3943. <https://doi.org/10.1021/bm700921h>.
- Nasto, L.A., Logroscino, C., 2016. *Cervical Spine, Cervical Spine Minimally Invasive and Open Surgery*. Springer International Publishing, Cham. <https://doi.org/10.1007/978-3-319-21608-9>.
- Nerurkar, N.L., Elliott, D.M., Mauck, R.L., 2010. Mechanical design criteria for intervertebral disc tissue engineering. *J. Biomech.* 43, 1017–1030. <https://doi.org/10.1016/j.jbiomech.2009.12.001>.
- Newell, N., Little, J.P., Christou, A., Adams, M.A., Adam, C.J., Masouros, S.D., 2017. Biomechanics of the human intervertebral disc: a review of testing techniques and results. *J. Mech. Behav. Biomed. Mater.* 69, 420–434. <https://doi.org/10.1016/j.jmbm.2017.01.037>.
- O'Connell, G.D., Vresilovic, E.J., Elliott, D.M., Connell, G.D.O., Vresilovic, E.J., Elliott, D.M., 2011. Human intervertebral disc internal strain in compression: the effect of disc region, loading position, and degeneration. *J. Orthop. Res.* 29, 547–555. <https://doi.org/10.1002/jor.21232>.
- Oh, S.H., Lee, J.H., 2013. Hydrophilization of synthetic biodegradable polymer scaffolds for improved cell/tissue compatibility. *Biomed. Mater.* 8, 014101 <https://doi.org/10.1088/1748-6041/8/1/014101>.
- Ohm, C., Brehmer, M., Zentel, R., 2010. Liquid crystalline elastomers as actuators and sensors. *Adv. Mater.* 22, 3366–3387. <https://doi.org/10.1002/adma.200904059>.
- Pham, M.H., Mehta, V.A., Tuchman, A., Hsieh, P.C., 2015. Material science in cervical total disc replacement. *BioMed Res. Int.* <https://doi.org/10.1155/2015/719123>, 2015.
- Prévôt, M.E., Andro, H., Alexander, S.L.M., Ustunel, S., Zhu, C., Nikolov, Z., Rafferty, S. T., Brannum, M.T., Kinsel, B., Korley, L.T.J., Freeman, E.J., McDonough, J.A., Clements, R.J., Hegmann, E., 2018. Liquid crystal elastomer foams with elastic properties specifically engineered as biodegradable brain tissue scaffolds. *Soft Matter* 14, 354–360. <https://doi.org/10.1039/c7sm01949a>.
- Prévôt, M.E., Ustunel, S., Bergquist, L.E., Cukelj, R., Gao, Y., Mori, T., Pauline, L., Clements, R.J., Hegmann, E., 2017. Synthesis of biocompatible liquid crystal elastomer foams as cell scaffolds for 3D spatial cell cultures. *JoVE* 1–11. <https://doi.org/10.3791/55452>.
- Rodríguez, A.G., Rodríguez-Soto, A.E., Burghardt, A.J., Berven, S., Majumdar, S., Lotz, J. C., 2012. Morphology of the human vertebral endplate. *J. Orthop. Res.* 30, 280–287. <https://doi.org/10.1002/jor.21513>.
- Rožič, B., Krause, S., Finkelmann, H., Cordoyiannis, G., Kutnjak, Z., 2010. Controlling the thermomechanical response of liquid-crystalline elastomers by influencing their critical behavior. *Appl. Phys. Lett.* 96, 2–4. <https://doi.org/10.1063/1.3358107>.
- Saed, M.O., Torbati, A.H., Nair, D.P., Yakacki, C.M., 2016. Synthesis of programmable main-chain liquid-crystalline elastomers using a two-stage thiol-acrylate reaction. *JoVE*. <https://doi.org/10.3791/53546>.
- Saed, M.O., Torbati, A.H., Starr, C.A., Visvanathan, R., Clark, N.A., Yakacki, C.M., 2017. Thiol-acrylate main-chain liquid-crystalline elastomers with tunable thermomechanical properties and actuation strain. *J. Polym. Sci., Part B: Polym. Phys.* 55, 157–168. <https://doi.org/10.1002/polb.24249>.
- Shang, Y., Wang, J., Ikeda, T., Jiang, L., Chem, J.M., Shang, Y., Wang, J., Ikeda, T., Jiang, L., 2019. Bio-inspired liquid crystal actuator materials. *J. Mater. Chem. C* 7, 3413–3428. <https://doi.org/10.1039/c9tc00107g>.
- Sharma, A., Mori, T., Mahnen, C.J., Everson, H.R., Leslie, M.T., Nielsen, A.D., Lussier, L., Zhu, C., Malcuit, C., Hegmann, T., McDonough, J.A., Freeman, E.J., Korley, L.T.J., Clements, R.J., Hegmann, E., 2017. Effects of structural variations on the cellular response and mechanical properties of biocompatible, biodegradable, and porous smectic liquid crystal elastomers. *Macromol. Biosci.* 17, 1600278. <https://doi.org/10.1002/mabi.201600278>.
- Sharma, A., Neshat, A., Mahnen, C.J., Nielsen, A.D., Snyder, J., Stankovich, T.L., Daum, B.G., Laspina, E.M., Beltrano, G., Gao, Y., Li, S., Park, B.W., Clements, R.J., Freeman, E.J., Malcuit, C., McDonough, J.A., Korley, L.T.J., Hegmann, T., Hegmann, E., 2015. Biocompatible, biodegradable and porous liquid crystal elastomer scaffolds for spatial cell cultures. *Macromol. Biosci.* 15, 200–214. <https://doi.org/10.1002/mabi.201400325>.
- Smith, K.E., Parks, S.S., Hyjek, M.A., Downey, S.E., Gall, K., 2009. The effect of the glass transition temperature on the toughness of photopolymerizable (meth)acrylate networks under physiological conditions. *Polymer* 50, 5112–5123. <https://doi.org/10.1016/j.polymer.2009.08.040>.
- Sun, Y., Amirrasouli, B., Razavi, S.B., Li, Q.M., Lowe, T., Withers, P.J., 2016. The variation in elastic modulus throughout the compression of foam materials. *Acta Mater.* 110, 161–174. <https://doi.org/10.1016/j.actamat.2016.03.003>.
- Thomsen, D.L., Keller, P., Naciri, J., Pink, R., Jeon, H., Shenoy, D., Ratna, B.R., 2001. Liquid crystal elastomers with mechanical properties of a muscle. *Macromolecules* 34, 5868–5875. <https://doi.org/10.1021/ma001639q>.
- Torbati, A.H., Mather, P.T., 2016. A hydrogel-forming liquid crystalline elastomer exhibiting soft shape memory. *J. Polym. Sci., Part B: Polym. Phys.* 54, 38–52. <https://doi.org/10.1002/polb.23892>.
- Torstick, F.B., Safranski, D.L., Burkus, J.K., Chappuis, J.L., Lee, C.S.D., Guldberg, R.E., Gall, K., Smith, K.E., 2017. Getting PEEK to stick to bone: the development of porous PEEK for interbody fusion devices. *Tech. Orthop.* 32, 158–166. <https://doi.org/10.1097/BTO.0000000000000242>.
- Traugott, N.A., Volpe, R.H., Bollinger, M.S., Saed, M.O., Torbati, A.H., Yu, K., Davivanyan, N., Yakacki, C.M., 2017. Liquid-crystal order during synthesis affects main-chain liquid-crystal elastomer behavior. *Soft Matter* 13, 7013–7025. <https://doi.org/10.1039/C7SM01405H>.
- Urayama, K., Honda, S., Takigawa, T., 2006. Slow dynamics of shape recovery of disordered nematic elastomers. *Phys. Rev. E - Stat. Nonlinear Soft Matter Phys.* 74, 1–7. <https://doi.org/10.1103/PhysRevE.74.041709>.
- Urayama, K., Kohmon, E., Kojima, M., Takigawa, T., 2009. Polydomain - monodomain transition of randomly disordered nematic elastomers with different cross-linking histories. *Macromolecules* 42, 4084–4089. <https://doi.org/10.1021/ma900469z>.
- Varanytsia, A., Nagai, H., Urayama, K., Palffy-Muhoray, P., 2015. Tunable lasing in cholesteric liquid crystal elastomers with accurate measurements of strain. *Sci. Rep.* 5, 2–9. <https://doi.org/10.1038/srep17739>.
- Verma, K., Gandhi, S.D., Maltenfort, M., Albert, T.J., Hilibrand, A.S., Vaccaro, A.R., Radcliff, K.E., 2013. Rate of adjacent segment disease in cervical disc arthroplasty versus single-level fusion. *Spine* 38, 2253–2257. <https://doi.org/10.1097/BRS.0000000000000052>. Phila. Pa. 1976.
- Volpe, R.H., Mistry, D., Patel, V.V., Patel, R.R., Yakacki, C.M., 2019. Dynamically crystallizing liquid-crystal elastomers for an expandable endplate-conforming interbody fusion cage. *Adv. Healthc. Mater.* 1901136. <https://doi.org/10.1002/adhm.201901136>, 1901136.
- Ware, T.H., McConney, M.E., Wie, J.J., Tondiglia, V.P., White, T.J., 2015. Voxelated liquid crystal elastomers. *Science* 347, 982–984. <https://doi.org/10.1126/science.1261019>, 80.
- Warner, M., Terentjev, E.M., 2003. *Liquid crystal elastomers*. Book 423. <https://doi.org/10.1017/CBO9781107415324.004>.
- Weilepp, J., Stein, P., Assfalg, N., Finkelmann, H., Martinoty, P., Brand, H.R., 1999. Rheological properties of mono- and polydomain liquid crystalline elastomers exhibiting a broad smectic A phase. *Europhys. Lett.* 47, 508–514. <https://doi.org/10.1209/epl/i1999-00417-3>.
- Yakacki, C.M., Saed, M., Nair, D.P., Gong, T., Reed, S.M., Bowman, C.N., 2015. Tailorable and programmable liquid-crystalline elastomers using a two-stage thiol-acrylate reaction. *RSC Adv.* 5, 18997–19001. <https://doi.org/10.1039/C5RA01039J>.